JCI The Journal of Clinical Investigation

Oncogene-induced matrix reorganization controls CD8$^+$ T cell function in the soft-tissue sarcoma microenvironment

Ashley M. Fuller, … , Sharon Gerecht, T.S. Karin Eisinger-Mathason

J Clin Invest. 2024. https://doi.org/10.1172/JCI167826.

Research In-Press Preview **Oncology**

CD8$^+$ T cell dysfunction impedes anti-tumor immunity in solid cancers but the underlying mechanisms are diverse and poorly understood. Extracellular matrix (ECM) composition has been linked to impaired T cell migration and enhanced tumor progression; however, impacts of individual ECM molecules on T cell function in the tumor microenvironment (TME) are only beginning to be elucidated. Upstream regulators of aberrant ECM deposition and organization in solid tumors are equally ill-defined. Therefore, we investigated how ECM composition modulates CD8$^+$ T cell function in undifferentiated pleomorphic sarcoma (UPS), an immunologically active desmoplastic tumor. Using an autochthonous murine model of UPS and data from multiple human patient cohorts, we discovered a multifaceted mechanism wherein the transcriptional co-activator YAP1 promotes collagen VI (COLVI) deposition in the UPS TME. In turn, COLVI induces CD8$^+$ T cell dysfunction and immune evasion by remodeling fibrillar collagen and inhibiting T cell autophagic flux. Unexpectedly, collagen I (COLI) opposed COLVI in this setting, promoting CD8$^+$ T cell function and acting as a tumor suppressor. Thus, CD8$^+$ T cell responses in sarcoma depend upon oncogene-mediated ECM composition and remodeling.

Oncogene-induced matrix reorganization controls CD8$^+$ T cell function in the soft-tissue sarcoma microenvironment

Ashley M. Fuller[1†], Hawley C. Pruitt[2†], Ying Liu[1], Valerie Irizarry-Negron[1], Hehai Pan[1], Hoogeun Song[1], Ann DeVine[1], Rohan Katti[1], Samir Devalaraja[1], Gabrielle E. Ciotti[1], Michael Gonzalez[3], Erik F. Williams[4], Ileana Murazzi[1], Dimitris Ntekoumes[2,5], Nicolas Skuli[1], Hakon Hakonarson[3], Daniel Zabransky[6], Jose Trevino[7], Ashani Weeraratna[6,8], Kristy Weber[9], Malay Haldar[1], Joseph A. Fraietta[4‡], Sharon Gerecht[2,5‡], T. S. Karin Eisinger-Mathason[1‡ *]

Affiliations

[1]Department of Pathology & Laboratory Medicine, Penn Sarcoma Program, Abramson Family Cancer Research Institute, Perelman School of Medicine, University of Pennsylvania, Philadelphia, PA, USA

[2]Department of Chemical and Biomolecular Engineering, The Institute for NanoBioTechnology, Johns Hopkins University, Baltimore, MD, USA

[3]Children's Hospital of Philadelphia, Philadelphia PA, USA

[4]Department of Microbiology, Center for Cellular Immunotherapies, Parker Institute for Cancer Immunotherapy, Perelman School of Medicine, University of Pennsylvania, Philadelphia, PA, USA

[5]Department of Biomedical Engineering, Duke University, Durham, NC, USA

[6]Department of Oncology, The Sidney Kimmel Cancer Center, Johns Hopkins School of Medicine, Baltimore, MD, USA

[7]Division of Surgical Oncology, Department of Surgery, Virginia Commonwealth University School of Medicine, Richmond, VA, USA

[8]Department of Biochemistry and Molecular Biology, Johns Hopkins Bloomberg School of Public Health, Baltimore, MD, USA

[9]Penn Sarcoma Program, Department of Orthopaedic Surgery, Perelman School of Medicine, University of Pennsylvania, Philadelphia, PA, USA

[†]Equally contributed. AMF and HCP can each list their name first on their respective CVs.

[‡]co-corresponding authors

***Correspondence should be addressed to:**

T.S. Karin Eisinger-Mathason

414 BRB II/III, 421 Curie Boulevard, University of Pennsylvania, Philadelphia, PA 19104-6160

Phone: 1-215-898-9086

Fax: 215-746-5511

E-mail: karineis@pennmedicine.upenn.edu

Conflicts of interest: The authors have declared that no conflict of interest exists.

ABSTRACT

$CD8^+$ T cell dysfunction impedes anti-tumor immunity in solid cancers but the underlying mechanisms are diverse and poorly understood. Extracellular matrix (ECM) composition has been linked to impaired T cell migration and enhanced tumor progression; however, impacts of individual ECM molecules on T cell function in the tumor microenvironment (TME) are only beginning to be elucidated. Upstream regulators of aberrant ECM deposition and organization in solid tumors are equally ill-defined. Therefore, we investigated how ECM composition modulates $CD8^+$ T cell function in undifferentiated pleomorphic sarcoma (UPS), an immunologically active desmoplastic tumor. Using an autochthonous murine model of UPS and data from multiple human patient cohorts, we discovered a multifaceted mechanism wherein the transcriptional co-activator YAP1 promotes collagen VI (COLVI) deposition in the UPS TME. In turn, COLVI induces $CD8^+$ T cell dysfunction and immune evasion by remodeling fibrillar collagen and inhibiting T cell autophagic flux. Unexpectedly, collagen I (COLI) opposed COLVI in this setting, promoting $CD8^+$ T cell function and acting as a tumor suppressor. Thus, $CD8^+$ T cell responses in sarcoma depend upon oncogene-mediated ECM composition and remodeling.

INTRODUCTION

Immunosuppression in the solid tumor microenvironment (TME) impedes T cell-mediated anti-tumor immunity. Tumors evade host adaptive immune responses by inducing $CD8^+$ T cell dysfunction, a hypofunctional state characterized by overexpression of inhibitory cell-surface receptors (e.g., PD1, TIM-3, LAG3), reduced effector function, and impaired proliferative capacity (1). Mechanisms underlying $CD8^+$ T cell dysfunction in solid cancers are of significant interest due to their impact on immunotherapy strategies. However, most studies in this field have focused on the roles of continuous antigen exposure/repetitive T cell receptor (TCR) stimulation, immune checkpoint-mediated inhibitory signaling, and immunosuppressive cytokines (2). Moreover, the importance of TME contexture in the setting of T cell-based therapies is poorly described. Thus, a more comprehensive and physiological evaluation of $CD8^+$ T cell dysfunction in solid tumors is critical for improving our understanding of immune evasion mechanisms in the TME and advancing actionable interventions.

Soft tissue sarcomas (STS) are heterogeneous solid mesenchymal tumors with ~70 distinct histologic subtypes (3). These lesions are characterized by mesenchymal gene expression, extensive extracellular matrix (ECM) deposition, and increased stiffness relative to normal tissues (4-6). Interestingly, these features are also observed in high-grade, poorly differentiated epithelial tumors where they are linked to progression, therapeutic resistance, and poor clinical outcomes (7). Recent studies have shown that the ECM facilitates cancer progression in part by inhibiting T cell migration/infiltration (8-11). However, the roles of individual ECM proteins in this process are only beginning to be defined. Moreover, little research has addressed the effects of ECM molecules on T cell function in solid tumors or identified upstream regulators of aberrant ECM deposition in this context. This paucity of available data indicates that further study, particularly in vivo, is necessary.

The 28 distinct molecular species of the collagen superfamily are some of the most abundant and diverse ECM constituents in normal and malignant tissues (12). Although the roles of specific collagen species in cancer-associated processes are ill-defined, a growing body of literature indicates that they can have context-specific functions in the TME. For example, type I collagen (ColI), a “prototypical” fibrillar collagen, promotes or is associated with malignant progression in some settings but has anti-tumor effects in others (13-17). These findings underscore the need to systematically interrogate the roles of individual collagens in specific tumor contexts, particularly with respect to their potential impacts on adaptive immunity.

Undifferentiated pleomorphic sarcoma (UPS) is a relatively common STS subtype that predominantly arises in adult skeletal muscle and has a 10-year survival rate of only ~25% (3, 18). Although some STS are considered immunologically “cold”, UPS patients have exhibited objective clinical responses to immune checkpoint inhibition in recent clinical trials (19, 20). These encouraging findings suggest that studies of UPS may provide valuable insights into strategies for enhancing T cell function and immunotherapy responses in solid tumors. Our previous work linked the intrinsic oncogenic functions of the transcriptional co-regulator Yes-associated protein 1 (YAP1), the central Hippo pathway effector, to UPS cell proliferation, tumor growth, and reduced human patient survival (21-24). However, we had not investigated the contribution of YAP1 to the UPS TME or immune cell activity. In some carcinomas, cancer cell-intrinsic YAP1 modulates macrophage and myeloid-derived suppressor cell recruitment and differentiation, suggesting an immunomodulatory role (25, 26). However, this observation has not been confirmed in mesenchymal cancers. YAP1 also possesses mechanosensory functions, and its nuclear localization and activity increase in response to stiff environments

such as those in tumor tissue (27). Therefore, herein, we interrogated the role of UPS cell-intrinsic YAP1 in the regulation of ECM deposition/organization and adaptive immune cell function in the TME. We discovered that YAP1 regulates ECM composition and cytotoxic T cell function, and that collagen type VI (ColVI), a microfibrillar collagen, indirectly modulates effector T cell function by opposing and remodeling ColI. We further identify COLVI as a putative diagnostic and survival biomarker in human UPS. Our findings implicate YAP1 inhibition, in combination with immunotherapy, as a promising approach to mitigate immune evasion in the sarcoma TME.

RESULTS

UPS cell-intrinsic Yap1 inhibits T cell activation and promotes CD8$^+$ T cell dysfunction

Using the genetically engineered mouse model (GEMM) of skeletal muscle UPS, *Kras*$^{G12D/+}$; *Trp53*$^{fl/fl}$ (KP) (28, 29), we previously showed that UPS cell-intrinsic Yap1 promotes tumorigenesis and progression by activating NF-κB (22). In this system, tumors are generated by injecting adenovirus-expressing Cre recombinase into the gastrocnemius muscle. Recombination initiates oncogenic *Kras* expression and deletes *Yap1*^{fl} alleles in infected muscle progenitor cells (28, 29). *TP53* mutations and deletion are prevalent in human UPS (30), as is MAPK hyperactivation downstream of KRAS (31). Consistent with our previous work (22), we observed significantly increased tumor latency and similar rates of tumor development when we introduced *Yap1*$^{fl/fl}$ alleles into the KP GEMM, creating *LSL-Kras*$^{G12D/+}$; *Trp53*$^{fl/fl}$; *Yap1*$^{fl/fl}$ (KPY) animals (**Figure 1A, B, Supp. Figure 1A**).

Our previous work has focused on mechanisms by which Yap1 impacts sarcoma cell-autonomous signaling and phenotypes such as proliferation, differentiation, and metastasis (21-23). Therefore, herein, we tested the hypothesis that UPS-cell intrinsic Yap1 also impacts the TME. To identify potential mechanisms of Yap1-mediated TME modulation, we explored a publicly available gene expression microarray dataset previously published by our group (22) comparing 5 unique KP and KPY bulk tumors. Loss of *Yap1* enhanced expression of numerous immune activation pathways, suggesting that UPS cell-intrinsic Yap1 is immunosuppressive (**Figure 1C**). To investigate how Yap1 controls immunosuppression in UPS, we performed flow cytometric and immunohistochemical (IHC) analyses of KP and KPY tumors. We did not detect changes in myeloid cell infiltration or polarization, or differences in B cell content (**Supp. Figure 1B-D**). However, we did observe increased proportions of CD44^{hi}CD8$^+$ and CD44^{hi}CD4$^+$ T cells in KPY relative to KP tumors, indicating enhanced T cell activation (**Figure 1D, E**). Furthermore, the percentage of dysfunctional effector CD8$^+$ T cells (CD39$^+$/Pd1$^+$

and Tim-3$^+$/Pd1$^+$) was higher in KP tumors vs. KPY (**Figure 1F, G**). Markers of central CD8$^+$ memory T cell differentiation (CD62L, CD127) remained unchanged (**Supp. Figure 2A**). Importantly, in KPY mice, the observed increases in T cell activation could not be attributed to reduced immunosuppressive Foxp3$^+$ T regulatory cell content, nor to enhanced T cell infiltration (**Supp. Figure 1B-D**). In fact, CD4$^+$ and CD8$^+$ T cell content was modestly decreased in KPY relative to KP tumors. Therefore, Yap1 may promote CD8$^+$ T cell dysfunction but likely does not impact T cell recruitment to the TME.

To further explore the relationship between Yap1$^+$ UPS cells and T cell activation, we evaluated levels of granzyme B (*Gzmb*), a T cell cytolysis marker, in GEMM tumors (**Figure 1H**). *Gzmb* expression (normalized to total T cells; *Cd3e*) was significantly increased in KPY vs. KP tumors, further demonstrating that Yap1$^+$ UPS cells are associated with immunosuppression. Therefore, to determine if UPS cell-intrinsic Yap1 modulates T cell effector function in addition to inhibitory receptor expression, we treated tumor-bearing KP and KPY mice with α-Pd1 or isotype control antibody. We hypothesized that immune checkpoint blockade would show increased efficacy in KPY animals due to enhanced T cell activation but have no effect in KP mice. Consistent with this hypothesis, time-to-maximum tumor volume was significantly increased in KPY animals, but not KP (**Figure 1I**). Notably, one KPY mouse experienced complete, durable tumor regression. We further evaluated the effect of YAP1$^+$ UPS cells on T cell function with human chimeric antigen receptor T (CART) cells that target the Tn glycoform of mucin 1 (TnMUC1 CART cells (32)). This neoantigen is expressed on human STS-109 cells, derived from a UPS patient tumor (**Supp. Figure 2B**). We co-cultured TnMUC1-CART cells with STS-109 cells expressing control or *YAP1*-specific shRNAs (shYAP1) at multiple effector:target ratios and analyzed longitudinal cytolysis (**Figure 1J, Supp. Figure 2C**). T cell cytolysis was enhanced in the presence of *YAP1*-deficient UPS cells, confirming that YAP1$^+$ UPS cells promote immunosuppression. To explore this data in a clinical context, we leveraged The Cancer Genome Atlas Sarcoma (TGCA-SARC) dataset (30). Consistent with our experimental findings, gene expression levels of T cell cytolysis markers (*GZMB* and perforin [*PRF1*]) in human UPS tumors were associated with improved survival (**Figure 1K, L**, **Supp. Figure 2D**) and negatively correlated with *YAP1* levels (**Figure 1M, N**). Thus, although some sarcomas are considered immunologically “cold”, our data suggest that cytotoxic T cell activation is a critical factor in UPS patient survival, and that modulating Yap1 and T cell activity may improve clinical outcomes.

UPS cell-intrinsic Yap1 promotes collagen VI deposition in the TME

We next sought to define the mechanism of crosstalk between Yap1$^+$ UPS cells and infiltrating CD8$^+$ T cells. Given recent studies in epithelial tumors showing that Yap1 can influence the cancer cell "secretome" (26, 33), we measured 31 cytokines and chemokines in sample supernatants from our CAR T cell cytolysis assays (**Figure 1J**). Many analytes were below the assay's lower limit of detection, but those we could detect were generally stable across samples (**Supp. Figure 3A, B**). These findings suggest that YAP1 likely does not control CD8$^+$ T cell function in the TME via cytokines or chemokines; thus, we focused on other potential mechanisms.

YAP1 is a known modulator of mechanosensing properties associated with ECM remodeling (34). Therefore, we investigated whether ECM-related processes underlie YAP1-mediated T cell suppression in the UPS TME. Using our microarray dataset of KP and KPY tumors to identify Yap1-dependent matrix genes, we found that many ECM- and tissue remodeling-associated pathways were altered in KPY tumors relative to KP (**Supp. Figure 3C**). We also observed that genes encoding many members of the collagen superfamily, particularly collagen type VI (ColVI; e.g., *Col6a1*, *Col6a2*, *Col6a3*), were downregulated in KPY relative to KP tumors (**Figure 2A, Supp. Figure 3D**). qRT-PCR and IHC analysis of bulk tumor specimens revealed that KPY tumors exhibited a trend toward reduced ColVI deposition overall (**Figure 2B, C**, **Supp. Figure 3E-H**). We did observe some heterogeneity in expression, potentially due to ColVI secretion by multiple cell types including macrophages (35) and UPS cells themselves; however, IHC analysis clearly showed that KPY tumors exhibited significantly less strong-positive (3+) and significantly more moderately positive (2+) staining than KP tumors (**Figure 2B, C**). We validated these findings in vitro with UPS cell lines derived from multiple unique KP GEMM tumors (KP230 and SKPY42.1 cells, referred to hereafter as "KP cells"). Specifically, KP cells transduced with one of multiple *Yap1*-specific shRNAs expressed substantially less Col6a1 and Col6a2 than control cells (**Figure 2D, E**). In contrast, we could not validate a role for Yap1 in the modulation of collagen type III expression (*Col3a1*; **Supp. Figure 3I**), nor that of other matrix genes such as fibronectin (*Fn1*; **Supp. Figure 3J**), indicating the potential specificity of this regulation.

To confirm the relationship between Yap1 and ColVI in UPS with a pharmacological approach, we treated tumor-bearing KP mice and KP cells in vitro with the histone deacetylase inhibitor (HDACi) Vorinostat (also known as Suberoylanilide Hydroxamic Acid; SAHA) and the BRD4 inhibitor JQ1, or vehicle control. We and others have reported that JQ1/SAHA (or other HDACi) combination treatment inhibits Yap1 expression in UPS

and other cancers (22, 36, 37). These studies confirmed that ColVI gene and protein expression were substantially downregulated in SAHA/JQ1-treated cells and tumors (**Figure 2F, G, Supp. Figure 3K-M**). Together, these data support the conclusion that UPS-cell intrinsic Yap1 promotes aberrant ColVI deposition in the TME, whereas genetic and non-specific pharmacologic inhibition of Yap1 can reverse this process.

As a transcriptional co-activator, Yap1 lacks a DNA-binding domain and must interact with Tea Domain (TEAD) transcription factors to stimulate gene expression; Tead1 is enriched in skeletal muscle tissue (38) and potentially muscle-derived tumors. Therefore, to explore the mechanism by which Yap1 promotes ColVI deposition, we leveraged publicly available Tead1 ChIP-seq data (GSE55186) from Yap1-driven embryonal rhabdomyosarcoma (eRMS) (39), skeletal muscle-derived tumors that lie on morphological and transcriptional continua with UPS (40). In murine Yap1-driven eRMS (39), Tead1-ChIP signal was enriched in a region that overlapped with the *Col6a1* 5' untranslated region (UTR), likely corresponding to the *Col6a1* promoter (**Supp. Figure 4A**). A second peak ~5 kb upstream of the *Col6a1* 5' UTR was also observed, potentially representing an enhancer region. Similarly, in cultured human eRMS cells (RD cells), TEAD1-ChIP signal was enriched ~9 kb upstream of the *COL6A1* 5' UTR (**Supp. Figure 4B**). These data suggest that transcriptionally active Yap1 upregulates ColVI deposition in skeletal muscle-derived sarcomas by directly stimulating *Col6a1* transcription.

Yap1-mediated ColVI deposition promotes CD8$^+$ T cell dysfunction

Based on our findings, we hypothesized that Yap1-mediated ColVI deposition in the UPS TME promotes CD8$^+$ T cell dysfunction. To test this idea, we developed a system wherein C57BL/6 KP cells (B6-KP cells) were seeded at 90% confluence and cultured under hypoxic conditions (1% O_2), stimulating them to deposit ECM. This ECM was then decellularized (decellularized ECM; dECM) and incubated with activated syngeneic C57BL/6 CD8$^+$ T cells (splenocytes) under normoxic conditions (21% O_2) (**Figure 2H**). dECMs were generated under hypoxic conditions because it is well-established that hypoxia stimulates robust ECM gene/protein expression and matrix remodeling in the TME (4, 7). Indeed, ColVI deposition was significantly increased in dECMs generated under hypoxia vs. normoxia (**Supp. Figure 4C, D**). Thus, UPS dECMs generated under hypoxic conditions were used in all experiments given our focus on Yap1-mediated ECM deposition and not the role of hypoxia vs. normoxia *per se*. Subsequent CD8$^+$ T cell culture on dECMs was conducted under normoxic conditions given previous

reports that hypoxia can either enhance or suppress $CD8^+$ T cell expansion and function depending on tissue/experimental context and extent of TCR stimulation (41-44).

To determine if Yap1-mediated ColVI deposition in UPS enhances T cell dysfunction, we generated dECMs from control and *Yap1*-deficient B6-KP cells. ColVI deposition was somewhat heterogeneous, but generally decreased in *Yap1*-deficient dECMs compared to controls, confirming the regulatory role of UPS cell-intrinsic Yap1 in ColVI secretion (**Figure 2I**). Although the observed reductions in ColVI were modest, these results were unsurprising because culturing cells at high confluence – which is required for matrix deposition in our system – is a well-established Yap1 suppressor (45), and can thereby minimize differences in Yap1 activity between shScr and shYap1 UPS cells. We cultured syngeneic $CD8^+$ T cells on these dECMs and measured the expression of T cell inhibitory receptors by flow cytometry. The proportion of $CD8^+$ T cells co-expressing Pd1 and Tim-3 was modestly reduced following culture on dECMs from *Yap1*-deficient compared to control UPS cells (**Supp. Figure 4E, F**). We also observed significantly higher percentages of $CD8^+$ T cells co-expressing the cytolytic markers IFNγ and TNFα following culture on dECMs from shYap1 cells (**Figure 2J**), consistent with the results of our CART-TnMUC1 assay (**Figure 1J)**. Together, these results support the conclusion that UPS cell-intrinsic Yap1 promotes $CD8^+$ T cell dysfunction.

We then determined the specific effects of ColVI, downstream of Yap1, on $CD8^+$ T cell surface marker expression by generating dECMs from ColVI-deficient KP cells (**Figure 3A**). In this assay, we targeted *Col6a1,* rather than other ColVI-encoding genes, because *Col6a1* is indispensable for ColVI protein synthesis (46). *Col6a1* depletion in KP cells significantly reduced $CD8^+$ T cell dysfunction in this assay, measured by Pd1/Tim-3 co-expression (**Figure 3B, C**). We also confirmed that ColVI depletion did not affect KP tumor-derived cell proliferation (**Supp. Figure 5A, B**), consistent with the hypothesis that the dominant role of ColVI is specific to immunomodulation in the TME. To directly test the effect of COLVI on T cell-mediated killing, we employed the human CART-TnMUC1 system introduced in **Figure 1J** (32). Longitudinal T cell-mediated cytolysis of STS-109 UPS cells expressing control or *COL6A1*-specific shRNAs revealed that COLVI depletion enhanced cytotoxic T cell function, phenocopying the effects of *YAP1* depletion (**Figure 3D, E**, **Supp. Figure 5C**). To address the possibility that shCOL6A1 UPS cells (and shYAP1 cells in **Figure 1J**) are simply more susceptible than shScr cells to T cell-mediated apoptosis, we treated them with recombinant human TNFα or IFNγ, two cytolytic cytokines known to be produced by $CD8^+$ T cells, and evaluated apoptosis by flow cytometry. We reasoned that

equivalent doses of purified cytokines should elicit similar levels of apoptosis in shYAP1/shCOL6A1 cells and controls if $CD8^+$ T cell function is truly enhanced in the setting of UPS cell-intrinsic *YAP1* or *COL6A1* deficiency. Purified cytokines did not increase shYAP1/shCOL6A1 UPS cell apoptosis relative to shScr controls, confirming enhanced CART cell cytotoxicity in the presence of reduced UPS cell-derived COLVI (**Supp. Figure 5D, E**). In fact, IFNγ reduced late apoptosis in shYAP1 and shCOL6A1 UPS cells compared to controls, albeit modestly and inconsistently across cytokine concentrations and independent shRNAs. Consistent with these results, COLVI protein was detected extracellularly and in UPS cell culture-conditioned medium (**Supp. Figure 5F-H**), where it can suppress CART-TnMUC1-mediated cytolysis and promote T cell dysfunction.

In light of our in vitro findings that ColVI suppresses $CD8^+$ T cell function, we investigated this relationship in vivo by generating control and *Col6a1* shRNA-expressing UPS tumors (syngeneic allograft of SKPY42.1 KP cells on a pure C57BL/6 background) in C57BL/6 hosts. In these immunocompetent mice, ColVI-deficient tumors were significantly smaller and slower growing than control tumors (**Figure 3F, G**). We demonstrated that ColVI-dependent tumor growth is mediated by T cell inactivation by depleting $CD8^+$ T cells in the syngeneic transplant system (**Figure 3H**, **Supp. Figure 5I**), where control and shCol6a1 tumors grew at the same rate. We also generated syngeneic orthotopic tumors by injecting control and shCol6a1-expressing KP cells into the gastrocnemius muscles of immunocompetent C57BL/6 mice (**Figure 3I**, **Supp. Figure 5J**). Flow cytometric analysis indicated that the proportion of $CD8^+$ T cells expressing dysfunction markers, including Tox, Tim-3, CD39, and Lag3, was significantly decreased in ColVI-deficient tumors compared to controls (**Figure 3J, K**). Together, these findings confirm that Yap1-mediated ColVI deposition in the UPS TME promotes $CD8^+$ T cell dysfunction and immune evasion.

ColVI colocalizes with and remodels ColI fibers in the UPS TME

Next, we explored the mechanism by which COLVI promotes $CD8^+$ T cell dysfunction in the UPS TME. We first asked whether $CD8^+$ T cell dysfunction is induced following direct interaction with deposited COLVI via known COLVI receptors. To test this hypothesis, we developed a second in vitro system by incorporating purified human COLVI into COLI-containing hydrogels. COLI, a fibrillar collagen, is a widely used hydrogel scaffold because of its mechanical stability, hydrophilicity, versatility, in vivo abundance, and ease of extraction (47). COLVI, which forms microfilaments instead of fibers, does not possess all of these properties and thus cannot be used to

generate hydrogels independently; moreover, unlike COLI, which can be found in isolation and need not interact with other matrix proteins in vivo, COLVI is always found bound to other ECM molecules and/or cell surface proteins (48). Activated human $CD8^+$ T cells were then cultured on these COLVI-containing hydrogels, allowing us to assess the impact of purified matrix proteins on $CD8^+$ T cells in a three-dimensional environment. Subsequently, we blocked the known COLVI receptors ITGB1, NG2/CSPG4, CMG2/ANTXR2, and ITGAV (**Supp. Figure 6A**). ITGAV and ITGB1 can bind multiple collagen species, including both COLVI and COLI; however, to our knowledge, NG2 and CMG2 are specific for COLVI (48-51). ITGB1 or NG2 neutralization with blocking antibodies did not affect $CD8^+$ T cell dysfunction (TIM-3/PD1 co-expression), nor did it restore $CD8^+$ T cell proliferation (KI67 positivity). Similar results were obtained following treatment of human $CD8^+$ T cells with cilengitide, a selective inhibitor of $\alpha v\beta 3$ and $\alpha v\beta 5$ integrins (52), and with activated $CD8^+$ T cells from *Cmg2*$^{-/-}$ mice (53) (**Supp. Figure 6B-F**). These results suggest that $CD8^+$ T cell dysfunction is not strongly modulated by canonical COLVI receptors. However, we cannot exclude the potential involvement of ITGAV and/or ITGB1, as neutralization of these receptors would likely block both T cell-COLVI and T cell-COLI interactions in our hydrogel system.

In the absence of a direct mechanism connecting ColVI receptors to T cell dysfunction, we investigated potential indirect mechanisms. ColVI binds to many ECM proteins, including ColI, one of the most abundant collagens in mammalian tissues (48, 54). In one study, COLI induced peripheral blood $CD8^+$ T cell proliferation in vitro when used in conjunction with CD3/TCR stimulation (55). Therefore, we hypothesized that Yap1-mediated ColVI deposition promotes $CD8^+$ T cell dysfunction by altering ColI content and/or organization in the UPS ECM. We first examined the effect of *Col6a1* depletion on ColI levels in KP cells in vitro, but generally observed no consistent changes in ColI gene or protein expression between *Col6a1*-deficient and control cells (**Supp. Figure 7A-G**). However, marked colocalization between ColI and ColVI in control (shScr) KP dECMs was observed, indicating a potential physical interaction between these two proteins (**Figure 4A, Supp. Figure 7H, Mov. S1-3**). Therefore, we considered the possibility that ColVI remodels ColI in the UPS TME, with potential implications for $CD8^+$ T cell function.

To test this hypothesis, we began by examining the architecture of fibrillar collagen molecules in explanted GEMM tumors. Using multiphoton second harmonic generation (SHG) imaging, we identified significant alterations to fibrillar collagen organization, including thinner and straighter fibers in KPY tumors

compared to KP (**Figure 4B-D**). Importantly, these changes in fibrillar collagen structure occurred despite similar levels of ColI gene expression and protein deposition in KP and KPY tumors (**Figure 2A**, **Supp. Figure 3D, 8A-C**). Similar results were observed in SAHA/JQ1-treated tumors compared to controls (**Supp. Figure 8D-F**). We also found that the fibrillar collagen structure of explanted human UPS tumors recapitulated that of KP tumors, confirming that our GEMMs successfully reproduce this aspect of UPS biology (**Figure 4E**, **Mov. S4-6**). To explore the impact of ColVI on ColI organization more directly, we examined extracellular ColI immunofluorescent staining patterns in control and *Col6a1*-deficient KP cell-derived ECMs (**Figure 4F**). In this experiment, matrices were not decellularized to circumvent the potential (albeit minor) changes in ECM structure induced by decellularization. ColI fibers in shCol6a1 ECMs were significantly longer, straighter, and wider than those in shScr ECMs, with significantly different orientation distributions, confirming ColVI-mediated remodeling (**Figure 4G-I, Supp. Figure 8G**). Finally, we asked whether COLVI alters COLI structure directly or indirectly through other mechanisms by performing SHG imaging of hydrogels containing purified COLI alone, or COLI together with purified COLVI (**Figure 4J**). As SHG only detects fibrillar collagen molecules, COLI, but not COLVI, is imaged in this assay. Remarkably, the addition of COLVI (250 μg/mL) to our hydrogel system nearly abolished the formation of COLI fibers and higher-level structures (e.g., fiber bundles; **Figure 4K**). In contrast, COLI fibers remained abundant in the presence of a different non-fibrillar collagen, collagen type IV (COLIV; also 250 μg/mL), underscoring the potential specificity of the COLI-COLVI relationship (**Figure 4L**). Therefore, we conclude that ColVI directly modifies ColI fiber architecture in the UPS TME.

ColI opposes ColVI and abrogates CD8$^+$ T cell dysfunction

We next sought to understand mechanistically how ColI-ColVI interactions impact CD8$^+$ T cells, hypothesizing that ColVI triggers dysfunction indirectly by remodeling ColI in the TME. To test the impact of ColI on CD8$^+$ T cell function, we incubated activated murine CD8$^+$ T cells on dECMs from control or *Col1a1*-deficient B6-KP cells. Unlike in the setting of *Yap1* and *Col6a1* deficiency (**Figure 2, 3**), the proportion of IFNγ^+TNFα^+ CD8$^+$ T cells was reduced following culture on *Col1a1*-deficient dECMs, indicating decreased cytolytic capacity (**Figure 5A, B**). We then cultured activated human CD8$^+$ T cells on hydrogels containing purified COLI alone, or COLI together with purified COLVI (**Figure 5C**). The proportion of PD1/TIM-3 co-expressing CD8$^+$ T cells was significantly reduced on COLI gels vs. COLVI-containing gels (**Figure 5D, E**); TIM-3 median fluorescence

intensity was similarly decreased (**Supp. Figure 9A**). Additionally, $CD8^+$ T cell proliferative capacity (KI67 positivity) was improved on COLI gels relative to COLI + COLVI gels (**Figure 5F, G**). The proportion of cytolytic $IFN\gamma^+TNF\alpha^+$ $CD8^+$ T cells was also modestly elevated in the presence of COLI alone (**Supp. Figure 9B**). We then tested the specificity of COLI-COLVI interactions on $CD8^+$ T cell function by substituting COLIV for COLVI in this assay. Remarkably, $CD8^+$ T cell dysfunction was not significantly impacted by the addition of COLIV to COLI-containing hydrogels (**Supp. Figure 9C**), consistent with our SHG data (**Figure 4L**), and further illustrating the specificity of the COLI-COLVI relationship.

The stiff, fibrotic microenvironments in desmoplastic solid tumors are well-known to activate Yap1 (27). Therefore, we ascertained whether COLVI drives $CD8^+$ T cell dysfunction by increasing ECM stiffness and potentiating Yap1 signaling. We queried Yap1 expression and subcellular localization in control, shCol6a1, and shCol1a1 KP cells, but did not detect significant differences in gene expression, protein levels, or S127 phosphorylation, an established surrogate for cytoplasmic retention and degradation (**Supp. Figure 9D-F**). Consistent with this observation, hydrogel stiffness was not significantly altered by the addition of COLVI (**Supp. Figure 9G**).

We also investigated the involvement of a ColI receptor, Lair1, in $CD8^+$ T cell dysfunction, given a recent report that Lair1 negatively regulates $CD8^+$ T cell activity and may promote immunotherapy resistance in lung cancer (56). Analysis of publicly available single-cell RNA-seq data from KP UPS tumors (GSE144507; (57)) demonstrated that *Lair1* was predominantly expressed on tumor-associated macrophages and minimally on $CD8^+$ T cells (**Supp. Figure 9H**). Moreover, *LAIR1* (but not *COL1A1* itself), was modestly associated with improved overall UPS patient survival (**Supp. Figure 9I, J**), inconsistent with its putative role promoting $CD8^+$ T cell immunosuppression (56). These results argue against the involvement of *Lair1* in UPS matrix-mediated immune evasion. Finally, we confirmed that neither molecular diffusion rates throughout, nor oxygen concentrations within, the hydrogel system were substantially impacted by the addition of COLVI, demonstrating that COLVI-induced $CD8^+$ T cell dysfunction in this model is not likely triggered by differential nutrient and/or oxygen availability (**Supp. Figure 9K, L**). Together, these observations clearly indicate that COLI abrogates COLVI-mediated $CD8^+$ T cell dysfunction, and demonstrate the relative importance of ECM signaling over Yap1 hyperactivation in this process.

Our findings thus far suggested that ColVI restrains ColI-mediated $CD8^+$ T cell activity and proliferation. To test this hypothesis in vivo, we generated subcutaneous syngeneic tumors by injecting SKPY42.1 cells expressing control, *Col1a1*-, or *Col6a1*-targeting shRNAs into C57BL/6 mice (**Figure 5H**). In this immunocompetent setting, *Col1a1*-deficient tumors grew more rapidly than both control and *Col6a1*-deficient tumors. Additionally, shCol1a1 and shScr tumors developed with similar efficiency (85% vs. 95%), whereas shCol6a1 tumors only formed in 46.2% of mice (**Figure 5I**). Of the shCol6a1 tumors that did form, 83.3% rapidly regressed before they reached 100 mm^3. Similar results were obtained in immunocompetent syngeneic orthotopic tumor models (**Supp. Figure 10A, B**). Importantly, shCol1a1-tumor-bearing mice experienced worse survival than mice bearing control tumors, whereas survival of shCol6a1-tumor bearing mice was improved (**Supp. Figure 10C**). Furthermore, Tim-3 and Tox were upregulated on $CD8^+$ T cells in *Col1a1*-deficient UPS tumors compared to controls (**Figure 5J, K**), indicating increased dysfunction due to ColI loss. Impressively, when we assessed the impact of *Col1a1* depletion on KP cell growth in vitro, *Col1a1*-deficient cells proliferated more slowly than controls, reflecting a discrepancy between ColI function in vitro and in vivo (**Supp. Figure 10D**). These results confirm that ColI in the UPS ECM controls tumor growth by enabling host anti-tumor immunity, whereas the aberrant deposition of ColVI opposes ColI and promotes immune evasion.

To ascertain whether ColVI or ColI plays the dominant role in matrix-mediated $CD8^+$ T cell dysfunction, we depleted *Col6a1* and *Col1a1* in the same population of SKPY42.1 cells and injected them into recipient syngeneic C57BL/6 mice (**Figure 5L, M**). Cells deficient for both collagens formed tumors at intermediate rates between those deficient for Col6a1 or Col1a1 individually (**Supp. Figure 10E**), but the resulting tumors (herein referred to as "double knockdown tumors") rapidly regressed before they reached ~100 mm^3 (**Figure 5N, Supp. Figure 10F**), phenocopying shCol6a1 tumors. To confirm T cell-dependent regression, we generated control and double knockdown tumors in nu/nu mice, in which mature T cells are lacking but innate immune cells are present. In this critical experiment, no significant differences in tumor formation or growth were observed (**Figure 5O, Supp. Figure 10G, H**), confirming T cell-mediated double knockdown tumor regression in the syngeneic model (**Figure 5N**). Thus, we conclude that ColVI is dominant over ColI in UPS matrix-mediated immune evasion.

ColVI promotes T cell dysfunction by disrupting $CD8^+$ T cell autophagic flux

To date, an immunosuppressive role of ColVI has not been documented in tumors. We therefore sought to identify the downstream mechanism by which ColVI deposition causes T cell dysfunction, and were intrigued by the reported ability of ColVI to modulate autophagy in fibroblasts and muscle tissue (58). Indeed, autophagy is a central regulator of T cell metabolism and essential for T cell activation (59). To assess whether ColVI impacted $CD8^+$ T cell autophagy, we encapsulated T cells in purified COLVI-containing hydrogels and visualized autophagosomes *in situ*. T cell autophagosomes were brighter and more numerous in the presence of COLVI vs. COLI alone (**Figure 6A-C**). To determine whether COLVI caused autophagosome accumulation by inducing autophagy, or by disrupting autophagic flux and autophagosome clearance, we treated activated $CD8^+$ T cells with chloroquine (CQ) in the presence or absence of COLVI and evaluated LC3B-II expression. In murine T cells, inhibiting autophagic flux with CQ did not further increase Lc3b-II, indicating that COLVI disrupts autophagic flux, but does not induce autophagy (**Figure 6D, E**). Activated human peripheral blood $CD8^+$ T cells generally showed the same trend (**Figure 6F-I**). We confirmed this result by staining for p62, a protein rapidly degraded during autophagy induction. In the presence of COLVI, p62 accumulated within T cells as evidenced by increased mean p62 signal intensity (**Figure 6J, K**). Together, these results indicate that extracellular COLVI inhibits $CD8^+$ T cell autophagic flux.

To explore the broader impacts of our findings, we next considered whether COLVI might also impact $CD8^+$ T cell function in other cancer types. Analysis of TCGA PanCancer RNA-seq data revealed that, like in sarcomas, *COL6A1*, *COL6A2*, and *COL6A3* are highly expressed in pancreatic ductal adenocarcinoma (PDAC) (**Supp. Figure 11A**). Indeed, PDAC tumors contain abundant desmoplastic stroma, secreted primarily by cancer-associated fibroblasts (CAFs) in the TME (14). Therefore, we generated dECMs from PDAC-CAFs isolated from three independent human tumors and confirmed their ability to secrete COLVI (**Supp. Figure 11B**). We then generated dECMs from control and shCOL6A1-expressing PDAC-CAFs and incubated them with activated human $CD8^+$ T cells. Surprisingly, the proportion of PD1/TIM-3-coexpressing $CD8^+$ T cells was not altered by exposure to *COL6A1*-deficient vs. -replete PDAC-CAF-derived matrix (**Supp. Figure 11C, D**). Thus, unlike in UPS, COLVI does not appear to modulate $CD8^+$ T cell function in PDAC. Given a recent report that fibroblast-derived ColI (containing Col1a1/Col1a2 heterotrimers) is distinct from PDAC cancer cell-derived ColI (containing Col1a1 homotrimers that possess oncogenic properties) (60), we then asked whether the differential immunomodulatory capacity of CAF-derived vs. UPS-derived ECM resulted from the production of heterotrimeric

vs. homotrimeric ColI, respectively. However, like fibroblasts (and unlike PDAC cancer cells) (60), *Col6a1*-sufficient and -deficient UPS cells secreted both Col1a1 and Col1a2 (**Supp. Figure 11E**), demonstrating that differential ColI trimer composition likely does not underlie the divergent effects of CAF-derived vs. UPS-derived matrix on $CD8^+$ T cell function. Taken together, these data underscore critical differences in matrix protein composition between sarcomas and carcinomas, and highlight the potential specificity of the ColVI-$CD8^+$ T cell relationship to mesenchymal tumors.

COLVI as a potential prognostic and diagnostic biomarker in human STS

To evaluate our experimental findings in a clinical context, we used data from multiple human UPS patient cohorts: the Detwiller et al. dataset (61), TCGA-SARC, and surgical specimens from the Hospital of the University of Pennsylvania (HUP). Like *YAP1* (22), *COL6A1*, *COL6A2*, and *COL6A3* were upregulated in human UPS relative to normal muscle tissue and correlated with poor patient outcomes (**Figure 7A-I**). Additionally, consistent with our in vitro and GEMM data demonstrating that Yap1 promotes ColVI deposition in the UPS TME, COLVI expression highly correlated with nuclear YAP1 staining, a surrogate for YAP1 transcriptional activity (**Figure 7J, K**). Moreover, the *COL6A1*, *COL6A2*, and *COL6A3* promoters appeared transcriptionally active in these specimens given the presence of H3K27Ac marks at these loci (**Figure 7L**). Finally, *COL6A3* gene expression positively tracked with that of *YAP1* and the *YAP1* target gene *FOXM1* (**Figure 7M, N**).

Finally, we explored the relationship between COLVI expression in UPS and other sarcoma subtypes using a tissue microarray (TMA). The mean UPS COLVI H-score (88.52; range: 105.73) was higher than that of all other subtypes, and significantly greater than leiomyosarcomas, neurofibromas, and synovial sarcomas (**Figure 8A, B**). Importantly, the dynamic range of COLVI staining in the UPS TMA cohort was similar to that in the HUP cohort (**Figure 7J-K**, range: 142.94). As UPS is more prevalent among older adults and presents with aggressive clinical features (18), we adjusted associations between COLVI H-score and histology for patient age, tumor grade, and tumor stage (**Figure 8A**). After controlling for these variables, relationships between COLVI H-score and histologic subtype were attenuated but remained statistically significant. Tumor grade was also significantly associated with COLVI H-score in univariate models. Furthermore, in TCGA-SARC, *COL6A1* gene expression was associated with reduced long-term survival among liposarcoma patients, where tumor COLVI expression levels are similar to those in UPS, but not among leiomyosarcoma patients, where tumor

COLVI levels are significantly lower (**Figure 8C, D**). Thus, COLVI expression may be a biomarker of clinical outcomes and immunotherapy sensitivity in some human sarcoma patients.

DISCUSSION

Until now, our understanding of the role of the ECM in anti-tumor immunity was primarily limited to its effects on leukocyte migration. Additionally, upstream mediators of aberrant ECM protein composition in the TME were poorly defined. Herein, we establish a more specific and mechanistic understanding of individual collagen molecules in the solid tumor ECM and their role in adaptive immunity (**Figure 8E**). We discovered that the highly expressed transcriptional co-regulator Yap1 promotes the deposition of a pro-tumor matrix protein, ColVI, in the UPS ECM. In turn, ColVI opposes anti-neoplastic ColI molecules in the TME, altering their organization/architecture, and disrupts $CD8^+$ T cell autophagic flux. Ultimately, this cascade facilitates $CD8^+$ T cell dysfunction by upregulating inhibitory receptors, suppressing proliferation, and reducing effector function. Together, our findings describe a non-canonical role of Yap1 in the TME and establish a direct mechanistic link between specific ECM constituents and modulation of immune cell function.

Despite the incredible diversity and abundance of collagen superfamily molecules in solid tumors (12, 17), the effects of specific collagens and other matrix proteins on T cell effector function in these contexts are only beginning to be characterized. For example, extracellular collagen molecules induced $CD8^+$ T cell exhaustion and attenuated responses to α-Pd1 checkpoint therapy in murine lung cancer models (56). These phenotypes were reversed following inhibition of LOXL2, a collagen cross-linking enzyme, but were not attributed to a specific collagen type, potentially because LOXL2 inhibition disrupts multiple collagen species. Additionally, laminin-111 has been implicated in the inhibition of $CD8^+$ T cell expansion and function in vitro; however, in vivo validation of these results has not been pursued (62). The authors did show that Matrigel, the primary component of which is laminin-111, may accelerate syngeneic mammary tumor growth in immunocompetent mice, but did not address whether Matrigel directly stimulates cancer cell proliferation in vivo (62). Furthermore, Robertson et al. (63) showed that COLIV may reduce T cell-mediated mammary carcinoma cell clearance, but did not establish a direct mechanistic link between COLIV and suppression of T cell function. Instead, the authors suggested that COLIV may induce a more immunosuppressive transcriptional/secretory profile in mammary carcinoma cells. However, because syngeneic mammary carcinoma cells and splenocytes were not used in this study (63), these

data are challenging to interpret. Conversely, herein, we uncovered specific immunomodulatory roles of two distinct collagen species in UPS and directly linked aberrant ECM composition/organization to induction of $CD8^+$ T cell dysfunction. Using multiple orthogonal in vitro and in vivo readouts, we discovered that ColVI and ColI possess opposing roles in this context, promoting and opposing immune evasion, respectively. The ColVI-mediated dysfunction program observed herein upregulated multiple T cell inhibitory receptors and dysfunction markers, suppressed $CD8^+$ T cell proliferation, and blunted $CD8^+$ T cell cytolytic capacity. In contrast, ColI was a tumor suppressor in vivo and reduced $CD8^+$ T cell dysfunction relative to ColVI. These observations are consistent with recent studies demonstrating the stimulatory effects of COLI on $CD8^+$ T cell function. For example, COLI co-stimulation enhanced peripheral blood-derived effector T cell expansion in vitro (55), and increased intratumoral T cell content and activation gene expression in PDAC models in vivo (15). In contrast, a study of three-dimensional culture models reported that high COLI density suppressed T cell proliferation, cytolytic marker gene expression, and cytolytic function (64). Taken together, these studies suggest that the effects of ColI on $CD8^+$ T cells are complex and potentially context-specific. Nevertheless, our study clearly shows that ColI is required for $CD8^+$ T cell function in UPS. By extension, stromal depletion strategies that reduce COLI deposition in the UPS TME could elicit detrimental outcomes.

One of the most intriguing findings from our study is that ColVI in the UPS TME directly remodels extracellular ColI. We suspect that this ColVI-mediated matrix remodeling masks binding motifs on ColI, such as RGD (Arg-Gly-Asp) sites or GXXGER consensus sequences, that would otherwise facilitate tumoricidal ColI-$CD8^+$ T cell interactions. However, the identity of the receptor on $CD8^+$ T cells mediating interactions with ColI in the UPS TME remains an open question. We excluded the possibility that Lair1 may be involved because it was not expressed on $CD8^+$ T cells in KP tumors. Similarly, the involvement of another ColI receptor, Ddr1, is unlikely, given Ddr1's previously reported role in the negative regulation of $CD8^+$ T cell migration/infiltration in carcinomas (65). Conversely, certain ColI-binding integrins such as Itga1, Itgav, and Itgb1 may be candidates given their putative roles promoting $CD8^+$ T activity (66-68), but are challenging to study in UPS because they bind to both ColI and ColVI (48-51). Therefore, careful biochemical studies are required to fully elucidate the mechanism by which ColI promotes $CD8^+$ T cell activity and inhibits immune evasion in UPS.

Senescence, functional exhaustion, insufficient homeostatic proliferation, deletion, and altered metabolism are all largely T cell-intrinsic mechanisms that can hamper endogenous and engineered T cell-

mediated anti-tumor immunity (1). Our findings offer an alternative model in which cancer cell-intrinsic biology drives failure of cytotoxic T cell activity by indirectly interfering with T cell autophagic flux. Autophagy is rapidly induced upon T cell activation, and the essential autophagy genes *Atg5* and *Atg7* are critical for mature T cell survival, activation, and expansion (69, 70). Moreover, disrupting T cell autophagic flux hinders clearance of damaged mitochondria, resulting in increased reactive oxygen species (ROS) generation and T cell apoptosis (70). Thus, whether and how aberrant ColVI deposition influences ROS production in T cells with dysregulated autophagic flux is an important direction for future research.

Our study has multiple implications for the clinical management of human UPS. First, as UPS is a diagnosis of exclusion, some pleomorphic neoplasms classified as "UPS" are more likely to be pseudosarcomas or other high-grade sarcomas (71). Thus, given the significantly increased COLVI levels in UPS relative to several other STS subtypes, COLVI may be a useful diagnostic biomarker for distinguishing UPS from other dedifferentiated pleomorphic tumors. Second, we found that Pd1 blockade extended survival of KPY mice, but not KP. Therefore, anti-Pd1 treatment was insufficient to reinvigorate dysfunctional effector T cells in KP mice, but did preserve $CD8^+$ T cells with robust cytolytic function in KPY. Finally, our findings show that Yap1 facilitates immune evasion by modulating TME composition and organization, and indicate that individual collagens may have unique or opposing effects on UPS patient responses to T cell-based therapies. Specifically, COLVI in the UPS ECM may suppress responses to immune checkpoint blockade, whereas COLI may potentiate efficacy. Thus, our study underscores the critical need to systematically evaluate the roles of individual ECM components in immunoregulation. Furthermore, our data specifically implicate YAP1 and/or COLVI targeting as promising strategies by which to improve the efficacy of checkpoint blockade and other T cell-based therapies in UPS, and potentially other desmoplastic solid tumors.

METHODS

Detailed methods are provided in the "Supplementary materials" file.

Sex as a biological variable

For GEMM studies, similar findings were observed in both sexes so results are reported for both together. Syngeneic transplant studies were performed in all females but the results are also expected to be relevant to

males. Data from TCGA-SARC and the sarcoma TMA are reported for both sexes together. HUP human specimens were completely deidentified.

Statistics

Analyses were performed using GraphPad Prism. Presentation of biological vs. technical replicates is indicated in the legends. Unless otherwise specified, in vitro experiments were replicated ≥3 times and data show mean ± SEM. Statistics are not shown for experiments with n < 3. Unpaired two-tailed t-tests and one-way ANOVAs were used to compare two or three group means, respectively. Two-way repeated-measures ANOVAs, mixed models, or non-linear regressions were used for in vivo tumor measurements. For correlations, Spearman's coefficient was used if at least one dataset was not normally distributed. Pearson's coefficient was used if both datasets were normally distributed. Shapiro-Wilk test was used to assess normality. $P<0.05$ was considered statistically significant. For Kaplan-Meier analyses of TCGA-SARC data, we pre-selected 4 gene expression cutoffs to identify the "optimal" cutoff for detecting gene-survival associations (72). Identical cutoffs were used in all analyses to avoid bias. The log-rank *P* values from each comparison were then adjusted for multiple comparisons using the two-stage linear step-up procedure of Benjamini, Krieger, and Yekutieli (false-discovery rate: 5%). All comparisons performed for each gene/survival endpoint combination and their associated adjusted *P* values are shown in **Supplementary Table 1**.

Study approval

All experiments were performed in accordance with NIH guidelines and approved by the UPenn Institutional Animal Care and Use Committee (approval #805758). Studies with human specimens were not considered human-subjects research (samples were de-identified and not collected exclusively for research).

Data availability

A "supporting data values" file is available in accordance with *JCI* policy. Additional data and materials are available from the corresponding author upon reasonable request.

AUTHOR CONTRIBUTIONS

AMF and HCP contributed equally. AMF's name is first because she coordinated all revision efforts with *JCI* while HCP pursued other professional opportunities. Other contributions include:

Conceptualization: TSKEM, SG, JAF, MH

Methodology: AMF, HCP YL, JAF

Validation: AMF, HCP, YL, VIN, HS, AD, RK, GEC, EFW, IM, NS

Formal Analysis: AMF, HCP, YL, RK, SD, GEC

Investigation: HCP, AMF, YL, VIN, HP, HS, AD, RK, SD, GEC, EFW, IM, DN, NS

Data Curation: AMF, YL, MG

Provision of resources: HH, DZ, JT, AW, KW, MH, JAF, SG, TSKEM

Writing-original draft preparation: AMF, HCP, TSKEM

Writing-review and editing: AMF, HCP, TSKEM

Visualization: AMF, HCP, YL, EFW, JAF, TSKEM

Supervision: MH, JAF, SG, TSKEM

Project administration: TSKEM

Funding acquisition: SG, TSKEM

ACKNOWLEDGEMENTS

We acknowledge Rebecca Gladdy, MD, for STS-109 cells, and Steven Leppla, PhD, for *Cmg2*$^{-/-}$cells. We also thank James Hayden and Frederick Keeney (Wistar Institute Imaging Facility) and Gordon Ruthel, PhD (PennVet Imaging Core) for assistance with multiphoton microscopy and analysis, and John Tobias, Ph.D., (UPenn Molecular Profiling Facility) for bioinformatic assistance. Lastly, we thank Martha Jordan, PhD, and Sydney Drury for assistance with in vivo flow cytometry, and Linnea T. Olsson, PhD, for assistance with molecular epidemiologic analysis of human sarcoma. We apologize to those we could not cite due to space constraints. **Funding:** The UPenn Abramson Cancer Center, The Penn Sarcoma Program, Steps to Cure Sarcoma, R01CA229688, The Johns Hopkins Physical Sciences–Oncology Center (U54CA210173), T32HL007971, DoD RA200237, and the American Cancer Society – Roaring Fork Valley Research Circle Postdoctoral Fellowship (PF-21-111-01-MM) provided funding. The UPenn Molecular Pathology and Imaging Core is supported by P30DK050306. The Penn Cytomics and Cell Sorting Shared Resource Laboratory is supported in part by P30016520 to the Abramson Cancer Center. Use of the PennVet Leica SP8 MP was made possible by S10OD021633-01. The UPenn Human Immunology Core is supported in part by P30AI045008 and P30CA016520.

REFERENCES

1. McLane LM, Abdel-Hakeem MS, and Wherry EJ. CD8 T Cell Exhaustion During Chronic Viral Infection and Cancer. *Annu Rev Immunol.* 2019;37:457-95.
2. Thommen DS, and Schumacher TN. T Cell Dysfunction in Cancer. *Cancer Cell.* 2018;33(4):547-62.
3. Fletcher CDM, World Health Organization., and International Agency for Research on Cancer. *WHO classification of tumours of soft tissue and bone.* Lyon: IARC Press; 2013.
4. Eisinger-Mathason TS, Zhang M, Qiu Q, Skuli N, Nakazawa MS, Karakasheva T, et al. Hypoxia-dependent modification of collagen networks promotes sarcoma metastasis. *Cancer Discov.* 2013;3(10):1190-205.
5. Pankova V, Thway K, Jones RL, and Huang PH. The Extracellular Matrix in Soft Tissue Sarcomas: Pathobiology and Cellular Signalling. *Front Cell Dev Biol.* 2021;9:763640.
6. Pepin K, Grimm R, Kargar S, Howe BM, Fritchie K, Frick M, et al. Soft Tissue Sarcoma Stiffness and Perfusion Evaluation by MRE and DCE-MRI for Radiation Therapy Response Assessment: A Technical Feasibility Study. *Biomed Phys Eng Express.* 2019;5(4).
7. Winkler J, Abisoye-Ogunniyan A, Metcalf KJ, and Werb Z. Concepts of extracellular matrix remodelling in tumour progression and metastasis. *Nat Commun.* 2020;11(1):5120.
8. Pruitt HC, Lewis D, Ciccaglione M, Connor S, Smith Q, Hickey JW, et al. Collagen fiber structure guides 3D motility of cytotoxic T lymphocytes. *Matrix Biol.* 2019.
9. Nicolas-Boluda A, Vaquero J, Vimeux L, Guilbert T, Barrin S, Kantari-Mimoun C, et al. Tumor stiffening reversion through collagen crosslinking inhibition improves T cell migration and anti-PD-1 treatment. *Elife.* 2021;10.
10. Pruitt HC, Guan Y, Liu H, Carey AE, Brennen WN, Lu J, et al. Collagen VI deposition mediates stromal T cell trapping through inhibition of T cell motility in the prostate tumor microenvironment. *Matrix Biol.* 2023;121:90-104.
11. Li L, Wei JR, Dong J, Lin QG, Tang H, Jia YX, et al. Laminin gamma2-mediating T cell exclusion attenuates response to anti-PD-1 therapy. *Sci Adv.* 2021;7(6).
12. Ricard-Blum S. The collagen family. *Cold Spring Harb Perspect Biol.* 2011;3(1):a004978.
13. Ozdemir BC, Pentcheva-Hoang T, Carstens JL, Zheng X, Wu CC, Simpson TR, et al. Depletion of carcinoma-associated fibroblasts and fibrosis induces immunosuppression and accelerates pancreas cancer with reduced survival. *Cancer Cell.* 2014;25(6):719-34.
14. Bhattacharjee S, Hamberger F, Ravichandra A, Miller M, Nair A, Affo S, et al. Tumor restriction by type I collagen opposes tumor-promoting effects of cancer-associated fibroblasts. *J Clin Invest.* 2021;131(11).
15. Chen Y, Kim J, Yang S, Wang H, Wu CJ, Sugimoto H, et al. Type I collagen deletion in alphaSMA(+) myofibroblasts augments immune suppression and accelerates progression of pancreatic cancer. *Cancer Cell.* 2021;39(4):548-65 e6.
16. Armstrong T, Packham G, Murphy LB, Bateman AC, Conti JA, Fine DR, et al. Type I collagen promotes the malignant phenotype of pancreatic ductal adenocarcinoma. *Clin Cancer Res.* 2004;10(21):7427-37.
17. Fuller AM, and Eisinger-Mathason TSK. Context Matters: Response Heterogeneity to Collagen-Targeting Approaches in Desmoplastic Cancers. *Cancers (Basel).* 2022;14(13).
18. Widemann BC, and Italiano A. Biology and Management of Undifferentiated Pleomorphic Sarcoma, Myxofibrosarcoma, and Malignant Peripheral Nerve Sheath Tumors: State of the Art and Perspectives. *J Clin Oncol.* 2018;36(2):160-7.
19. Tawbi HA, Burgess M, Bolejack V, Van Tine BA, Schuetze SM, Hu J, et al. Pembrolizumab in advanced soft-tissue sarcoma and bone sarcoma (SARC028): a multicentre, two-cohort, single-arm, open-label, phase 2 trial. *Lancet Oncol.* 2017;18(11):1493-501.
20. Keung EZ, Lazar AJ, Torres KE, Wang WL, Cormier JN, Ashleigh Guadagnolo B, et al. Phase II study of neoadjuvant checkpoint blockade in patients with surgically resectable undifferentiated pleomorphic sarcoma and dedifferentiated liposarcoma. *BMC Cancer.* 2018;18(1):913.
21. Ye S, Liu Y, Fuller AM, Katti R, Ciotti GE, Chor S, et al. TGFbeta and Hippo Pathways Cooperate to Enhance Sarcomagenesis and Metastasis through the Hyaluronan-Mediated Motility Receptor (HMMR). *Mol Cancer Res.* 2020.
22. Ye S, Lawlor MA, Rivera-Reyes A, Egolf S, Chor S, Pak K, et al. YAP1-mediated suppression of USP31 enhances NF-kappaB activity to promote sarcomagenesis. *Cancer Res.* 2018.

23. Rivera-Reyes A, Ye S, G EM, Egolf S, G EC, Chor S, et al. YAP1 enhances NF-kappaB-dependent and independent effects on clock-mediated unfolded protein responses and autophagy in sarcoma. *Cell Death Dis.* 2018;9(11):1108.
24. Eisinger-Mathason TS, Mucaj V, Biju KM, Nakazawa MS, Gohil M, Cash TP, et al. Deregulation of the Hippo pathway in soft-tissue sarcoma promotes FOXM1 expression and tumorigenesis. *Proc Natl Acad Sci U S A.* 2015;112(26):E3402-11.
25. Murakami S, Shahbazian D, Surana R, Zhang W, Chen H, Graham GT, et al. Yes-associated protein mediates immune reprogramming in pancreatic ductal adenocarcinoma. *Oncogene.* 2017;36(9):1232-44.
26. Wang G, Lu X, Dey P, Deng P, Wu CC, Jiang S, et al. Targeting YAP-Dependent MDSC Infiltration Impairs Tumor Progression. *Cancer Discov.* 2016;6(1):80-95.
27. Elosegui-Artola A, Andreu I, Beedle AEM, Lezamiz A, Uroz M, Kosmalska AJ, et al. Force Triggers YAP Nuclear Entry by Regulating Transport across Nuclear Pores. *Cell.* 2017;171(6):1397-410 e14.
28. Kirsch DG, Dinulescu DM, Miller JB, Grimm J, Santiago PM, Young NP, et al. A spatially and temporally restricted mouse model of soft tissue sarcoma. *Nat Med.* 2007;13(8):992-7.
29. Mito JK, Riedel RF, Dodd L, Lahat G, Lazar AJ, Dodd RD, et al. Cross species genomic analysis identifies a mouse model as undifferentiated pleomorphic sarcoma/malignant fibrous histiocytoma. *PLoS One.* 2009;4(11):e8075.
30. Cancer Genome Atlas Research Network. Electronic address edsc, and Cancer Genome Atlas Research N. Comprehensive and Integrated Genomic Characterization of Adult Soft Tissue Sarcomas. *Cell.* 2017;171(4):950-65 e28.
31. Serrano C, Romagosa C, Hernandez-Losa J, Simonetti S, Valverde C, Moline T, et al. RAS/MAPK pathway hyperactivation determines poor prognosis in undifferentiated pleomorphic sarcomas. *Cancer.* 2016;122(1):99-107.
32. Posey AD, Jr., Schwab RD, Boesteanu AC, Steentoft C, Mandel U, Engels B, et al. Engineered CAR T Cells Targeting the Cancer-Associated Tn-Glycoform of the Membrane Mucin MUC1 Control Adenocarcinoma. *Immunity.* 2016;44(6):1444-54.
33. Marquard S, Thomann S, Weiler SME, Bissinger M, Lutz T, Sticht C, et al. Yes-associated protein (YAP) induces a secretome phenotype and transcriptionally regulates plasminogen activator Inhibitor-1 (PAI-1) expression in hepatocarcinogenesis. *Cell Commun Signal.* 2020;18(1):166.
34. Low BC, Pan CQ, Shivashankar GV, Bershadsky A, Sudol M, and Sheetz M. YAP/TAZ as mechanosensors and mechanotransducers in regulating organ size and tumor growth. *FEBS Lett.* 2014;588(16):2663-70.
35. Schnoor M, Cullen P, Lorkowski J, Stolle K, Robenek H, Troyer D, et al. Production of type VI collagen by human macrophages: a new dimension in macrophage functional heterogeneity. *J Immunol.* 2008;180(8):5707-19.
36. Lin CH, Kuo JC, Li D, Koenig AB, Pan A, Yan P, et al. AZD5153, a Bivalent BRD4 Inhibitor, Suppresses Hepatocarcinogenesis by Altering BRD4 Chromosomal Landscape and Modulating the Transcriptome of HCC Cells. *Front Cell Dev Biol.* 2022;10:853652.
37. Zanconato F, Battilana G, Forcato M, Filippi L, Azzolin L, Manfrin A, et al. Transcriptional addiction in cancer cells is mediated by YAP/TAZ through BRD4. *Nat Med.* 2018;24(10):1599-610.
38. Stewart AF, Richard CW, 3rd, Suzow J, Stephan D, Weremowicz S, Morton CC, et al. Cloning of human RTEF-1, a transcriptional enhancer factor-1-related gene preferentially expressed in skeletal muscle: evidence for an ancient multigene family. *Genomics.* 1996;37(1):68-76.
39. Tremblay AM, Missiaglia E, Galli GG, Hettmer S, Urcia R, Carrara M, et al. The Hippo transducer YAP1 transforms activated satellite cells and is a potent effector of embryonal rhabdomyosarcoma formation. *Cancer Cell.* 2014;26(2):273-87.
40. Rubin BP, Nishijo K, Chen HI, Yi X, Schuetze DP, Pal R, et al. Evidence for an unanticipated relationship between undifferentiated pleomorphic sarcoma and embryonal rhabdomyosarcoma. *Cancer Cell.* 2011;19(2):177-91.
41. Vuillefroy de Silly R, Dietrich PY, and Walker PR. Hypoxia and antitumor CD8(+) T cells: An incompatible alliance? *Oncoimmunology.* 2016;5(12):e1232236.
42. Gropper Y, Feferman T, Shalit T, Salame TM, Porat Z, and Shakhar G. Culturing CTLs under Hypoxic Conditions Enhances Their Cytolysis and Improves Their Anti-tumor Function. *Cell Rep.* 2017;20(11):2547-55.

43. Scharping NE, Rivadeneira DB, Menk AV, Vignali PDA, Ford BR, Rittenhouse NL, et al. Mitochondrial stress induced by continuous stimulation under hypoxia rapidly drives T cell exhaustion. *Nat Immunol.* 2021;22(2):205-15.
44. Bannoud N, Dalotto-Moreno T, Kindgard L, Garcia PA, Blidner AG, Marino KV, et al. Hypoxia Supports Differentiation of Terminally Exhausted CD8 T Cells. *Front Immunol.* 2021;12:660944.
45. Zhao B, Wei X, Li W, Udan RS, Yang Q, Kim J, et al. Inactivation of YAP oncoprotein by the Hippo pathway is involved in cell contact inhibition and tissue growth control. *Genes Dev.* 2007;21(21):2747-61.
46. Bonaldo P, Braghetta P, Zanetti M, Piccolo S, Volpin D, and Bressan GM. Collagen VI deficiency induces early onset myopathy in the mouse: an animal model for Bethlem myopathy. *Hum Mol Genet.* 1998;7(13):2135-40.
47. Sarrigiannidis SO, Rey JM, Dobre O, Gonzalez-Garcia C, Dalby MJ, and Salmeron-Sanchez M. A tough act to follow: collagen hydrogel modifications to improve mechanical and growth factor loading capabilities. *Mater Today Bio.* 2021;10:100098.
48. Cescon M, Gattazzo F, Chen P, and Bonaldo P. Collagen VI at a glance. *J Cell Sci.* 2015;128(19):3525-31.
49. Burgi J, Abrami L, Castanon I, Abriata LA, Kunz B, Yan SE, et al. Ligand Binding to the Collagen VI Receptor Triggers a Talin-to-RhoA Switch that Regulates Receptor Endocytosis. *Dev Cell.* 2020;53(4):418-30 e4.
50. Davis GE. Affinity of integrins for damaged extracellular matrix: alpha v beta 3 binds to denatured collagen type I through RGD sites. *Biochem Biophys Res Commun.* 1992;182(3):1025-31.
51. Zeltz C, and Gullberg D. The integrin-collagen connection - a glue for tissue repair? *J Cell Sci.* 2016;129(6):1284.
52. Mas-Moruno C, Rechenmacher F, and Kessler H. Cilengitide: the first anti-angiogenic small molecule drug candidate design, synthesis and clinical evaluation. *Anticancer Agents Med Chem.* 2010;10(10):753-68.
53. Liu S, Crown D, Miller-Randolph S, Moayeri M, Wang H, Hu H, et al. Capillary morphogenesis protein-2 is the major receptor mediating lethality of anthrax toxin in vivo. *Proc Natl Acad Sci U S A.* 2009;106(30):12424-9.
54. Keene DR, Ridgway CC, and Iozzo RV. Type VI microfilaments interact with a specific region of banded collagen fibrils in skin. *J Histochem Cytochem.* 1998;46(2):215-20.
55. Rao WH, Hales JM, and Camp RD. Potent costimulation of effector T lymphocytes by human collagen type I. *J Immunol.* 2000;165(9):4935-40.
56. Peng DH, Rodriguez BL, Diao L, Chen L, Wang J, Byers LA, et al. Collagen promotes anti-PD-1/PD-L1 resistance in cancer through LAIR1-dependent CD8(+) T cell exhaustion. *Nat Commun.* 2020;11(1):4520.
57. Devalaraja S, To TKJ, Folkert IW, Natesan R, Alam MZ, Li M, et al. Tumor-Derived Retinoic Acid Regulates Intratumoral Monocyte Differentiation to Promote Immune Suppression. *Cell.* 2020;180(6):1098-114 e16.
58. Castagnaro S, Chrisam M, Cescon M, Braghetta P, Grumati P, and Bonaldo P. Extracellular Collagen VI Has Prosurvival and Autophagy Instructive Properties in Mouse Fibroblasts. *Front Physiol.* 2018;9:1129.
59. Botbol Y, Guerrero-Ros I, and Macian F. Key roles of autophagy in regulating T-cell function. *Eur J Immunol.* 2016;46(6):1326-34.
60. Chen Y, Yang S, Tavormina J, Tampe D, Zeisberg M, Wang H, et al. Oncogenic collagen I homotrimers from cancer cells bind to alpha3beta1 integrin and impact tumor microbiome and immunity to promote pancreatic cancer. *Cancer Cell.* 2022;40(8):818-34 e9.
61. Detwiller KY, Fernando NT, Segal NH, Ryeom SW, D'Amore PA, and Yoon SS. Analysis of hypoxia-related gene expression in sarcomas and effect of hypoxia on RNA interference of vascular endothelial cell growth factor A. *Cancer Res.* 2005;65(13):5881-9.
62. Liu X, Qiao Y, Chen J, and Ge G. Basement membrane promotes tumor development by attenuating T cell activation. *J Mol Cell Biol.* 2022;14(2).
63. Robertson C, Sebastian A, Hinckley A, Rios-Arce ND, Hynes WF, Edwards SA, et al. Extracellular matrix modulates T cell clearance of malignant cells in vitro. *Biomaterials.* 2022;282:121378.
64. Kuczek DE, Larsen AMH, Thorseth ML, Carretta M, Kalvisa A, Siersbaek MS, et al. Collagen density regulates the activity of tumor-infiltrating T cells. *J Immunother Cancer.* 2019;7(1):68.

65. Sun X, Wu B, Chiang HC, Deng H, Zhang X, Xiong W, et al. Tumour DDR1 promotes collagen fibre alignment to instigate immune exclusion. *Nature.* 2021;599(7886):673-8.
66. Bromley SK, Akbaba H, Mani V, Mora-Buch R, Chasse AY, Sama A, et al. CD49a Regulates Cutaneous Resident Memory CD8(+) T Cell Persistence and Response. *Cell Rep.* 2020;32(9):108085.
67. Malenica I, Adam J, Corgnac S, Mezquita L, Auclin E, Damei I, et al. Integrin-alpha(V)-mediated activation of TGF-beta regulates anti-tumour CD8 T cell immunity and response to PD-1 blockade. *Nat Commun.* 2021;12(1):5209.
68. Nicolet BP, Guislain A, van Alphen FPJ, Gomez-Eerland R, Schumacher TNM, van den Biggelaar M, et al. CD29 identifies IFN-gamma-producing human CD8(+) T cells with an increased cytotoxic potential. *Proc Natl Acad Sci U S A.* 2020;117(12):6686-96.
69. Pua HH, Dzhagalov I, Chuck M, Mizushima N, and He YW. A critical role for the autophagy gene Atg5 in T cell survival and proliferation. *J Exp Med.* 2007;204(1):25-31.
70. Pua HH, Guo J, Komatsu M, and He YW. Autophagy is essential for mitochondrial clearance in mature T lymphocytes. *J Immunol.* 2009;182(7):4046-55.
71. Goldblum JR. An approach to pleomorphic sarcomas: can we subclassify, and does it matter? *Mod Pathol.* 2014;27 Suppl 1:S39-46.
72. Eng KH, Schiller E, and Morrell K. On representing the prognostic value of continuous gene expression biomarkers with the restricted mean survival curve. *Oncotarget.* 2015;6(34):36308-18.

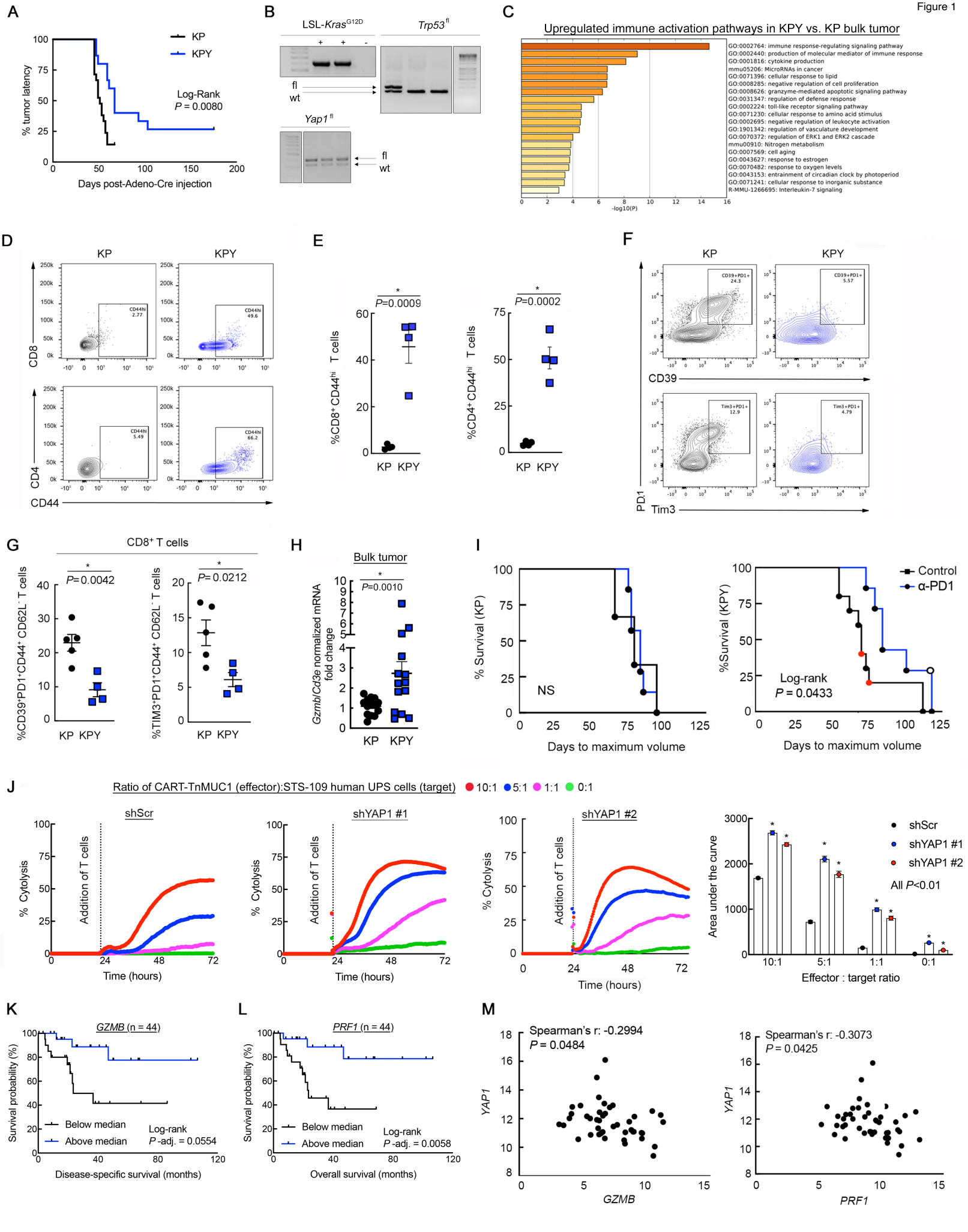
A
KP
KPY
Log-Rank
P = 0.0080
% tumor latency
Days post-Adeno-Cre injection
B
LSL-KrasG12D
Trp53fl
Yap1fl
fl
wt
C
Upregulated immune activation pathways in KPY vs. KP bulk tumor
GO:0002764: immune response-regulating signaling pathway
GO:0002440: production of molecular mediator of immune response
GO:0001816: cytokine production
mmu05206: MicroRNAs in cancer
GO:0071396: cellular response to lipid
GO:0008285: negative regulation of cell proliferation
GO:0008626: granzyme-mediated apoptotic signaling pathway
GO:0031347: regulation of defense response
GO:0002224: toll-like receptor signaling pathway
GO:0071230: cellular response to amino acid stimulus
GO:0002695: negative regulation of leukocyte activation
GO:1901342: regulation of vasculature development
GO:0070372: regulation of ERK1 and ERK2 cascade
mmu00910: Nitrogen metabolism
GO:0007569: cell aging
GO:0043627: response to estrogen
GO:0070482: response to oxygen levels
GO:0043153: entrainment of circadian clock by photoperiod
GO:0071241: cellular response to inorganic substance
R-MMU-1266695: Interleukin-7 signaling
-log10(P)
D
KP
KPY
CD8
CD4
CD44
E
P=0.0009
P=0.0002
%CD8+CD44hi T cells
%CD4+CD44hi T cells
F
CD39
PD1
Tim3
G
CD8+ T cells
P=0.0042
P=0.0212
%CD39+PD1+CD44+ CD62L- T cells
%TIM3+PD1+CD44+ CD62L- T cells
H
Bulk tumor
P=0.0010
Gzmb/Cd3e normalized mRNA fold change
I
% Survival (KP)
NS
Days to maximum volume
%Survival (KPY)
Control
α-PD1
Log-rank
P = 0.0433
J
Ratio of CART-TnMUC1 (effector):STS-109 human UPS cells (target)
10:1
5:1
1:1
0:1
shScr
shYAP1 #1
shYAP1 #2
% Cytolysis
Addition of T cells
Time (hours)
Area under the curve
All P<0.01
Effector : target ratio
K
GZMB (n = 44)
Survival probability (%)
Below median
Above median
Log-rank
P -adj. = 0.0554
Disease-specific survival (months)
L
PRF1 (n = 44)
Log-rank
P -adj. = 0.0058
Overall survival (months)
M
Spearman's r: -0.2994
P = 0.0484
Spearman's r: -0.3073
P = 0.0425
YAP1
GZMB
PRF1

Figure 1. YAP1$^+$ UPS cells inhibit CD8$^+$ T cell activation and promote dysfunction. (**A**) Kaplan-Meier latency curves of KP and KPY UPS tumors (n >10 per genotype). (**B**) Validation of genotypes from **A** (fl: floxed; wt: wild-type). The *Trp53*^{fl} and *Yap1*^{fl} bands and their respective ladders are from the same gels but were separated for presentation. (**C**) Metascape pathway analysis of 5 unique bulk KP and KPY tumors. Includes all genes with >2-fold expression increase in KPY vs. KP, identified via microarrays. (**D, E**) Representative contour plots (**D**) and quantification (**E**) of CD8$^+$CD44^{hi} and CD4$^+$CD44^{hi} T cells in KP and KPY tumors. (**F, G**) Representative contour plots (**F**) and quantification (**G**) of CD39, Tim-3, and Pd1 expression in CD8$^+$ T cells from KP and KPY tumors. For **E** and **G**, points represent individual tumors; two-tailed unpaired t-tests. (**H**) *Gzmb* qRT-PCR in bulk KP and KPY tumors; two-tailed unpaired t-test. (**I**) Kaplan-Meier survival curves of KP and KPY mice treated with α-Pd1 or control. Red and black circles in control curves indicate IgG- and un-injected mice, respectively. Open circle: mouse with durable tumor regression. X-axis: days since adeno Cre injection. (**J**) Average longitudinal cytolysis of shScr or shYAP1 human STS-109 UPS cells during co-culture with CART-TnMUC1 cells from three independent human donors. Measurements indicate % target (UPS) cell cytolysis. Quantification: one-way ANOVA with Dunnett's (vs. shScr) for each ratio. Points for individual replicates overlap. shScr data are identical to those in **Fig. 3D-E** (performed in the same experiment). (**K**, **L**) Kaplan-Meier survival curves of UPS patients in TCGA-SARC stratified by intratumoral *GZMB* (**K**) and *PRF1* (**L**) expression. (**M**, **N**) Correlation of *YAP1* with *GZMB* (**M**) and *PRF1* (**N**) gene expression in UPS tumors from TCGA-SARC.

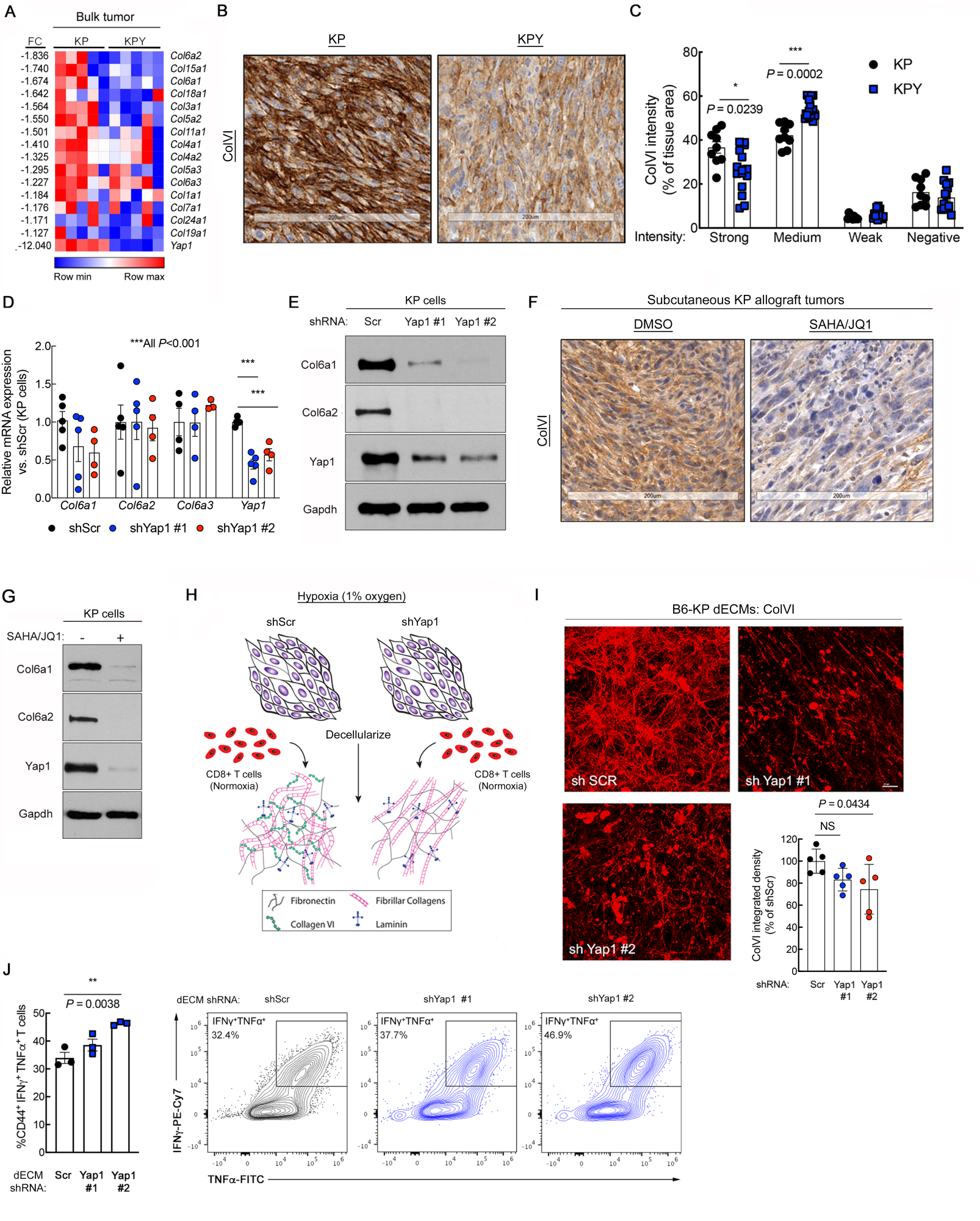
A
Bulk tumor
FC
KP
KPY
-1.836 Col6a2
-1.740 Col15a1
-1.674 Col6a1
-1.642 Col18a1
-1.564 Col3a1
-1.550 Col5a2
-1.501 Col11a1
-1.410 Col4a1
-1.325 Col4a2
-1.295 Col5a3
-1.227 Col6a3
-1.184 Col1a1
-1.176 Col7a1
-1.171 Col24a1
-1.127 Col19a1
-12.040 Yap1
Row min
Row max
B
KP
KPY
ColVI
200um
C
ColVI intensity (% of tissue area)
*
P = 0.0239
***
P = 0.0002
KP
KPY
Intensity:
Strong
Medium
Weak
Negative
D
***All P<0.001
Relative mRNA expression vs. shScr (KP cells)
***
***
Col6a1
Col6a2
Col6a3
Yap1
shScr
shYap1 #1
shYap1 #2
E
KP cells
shRNA:
Scr
Yap1 #1
Yap1 #2
Col6a1
Col6a2
Yap1
Gapdh
F
Subcutaneous KP allograft tumors
DMSO
SAHA/JQ1
ColVI
200um
G
KP cells
SAHA/JQ1:
-
+
Col6a1
Col6a2
Yap1
Gapdh
H
Hypoxia (1% oxygen)
shScr
shYap1
Decellularize
CD8+ T cells (Normoxia)
CD8+ T cells (Normoxia)
Fibronectin
Fibrillar Collagens
Collagen VI
Laminin
I
B6-KP dECMs: ColVI
sh SCR
sh Yap1 #1
sh Yap1 #2
P = 0.0434
NS
ColVI integrated density (% of shScr)
shRNA:
Scr
Yap1 #1
Yap1 #2
J
**
P = 0.0038
%CD44+ IFNγ+ TNFα+ T cells
dECM shRNA:
Scr
Yap1 #1
Yap1 #2
dECM shRNA:
shScr
shYap1 #1
shYap1 #2
IFNγ+TNFα+
32.4%
IFNγ+TNFα+
37.7%
IFNγ+TNFα+
46.9%
IFNγ-PE-Cy7
TNFα-FITC

Figure 2. UPS-cell intrinsic Yap1 mediates collagen VI (ColVI) deposition in the TME. (**A**) Heat map of gene expression microarray data comparing 5 unique KP and KPY bulk tumors. The top 1/3 of collagen-encoding genes modulated by *Yap1* deletion is displayed. **Supp. Figure 3D** shows the remaining 2/3 of collagen-encoding genes. FC = fold change. (**B, C**) Representative images (**B**) and quantification (**C**) of ColVI IHC in KP and KPY tumors. Two-tailed unpaired t-tests with Welch correction and Holm-Sidak multiple comparisons test (n = 3-5 mice per genotype with 3 sections per mouse). (**D**) qRT-PCR of *Col6a1*, *Col6a2*, *Col6a3,* and *Yap1* gene expression in KP cells expressing a control or one of multiple independent *Yap1*-targeting shRNAs. One-way ANOVA with Dunnett's (vs. shScr) for each gene. (**E**) Representative immunoblot of KP cells treated as in **D**. (**F**) Representative images of ColVI IHC in KP tumor-bearing mice treated with 25 mg/kg SAHA + 50 mg/kg JQ1 or vehicle control for 20 days. Quantification is in **Supp. Figure 3M**. (**G**) Representative immunoblot of KP cells treated with SAHA (2 μM) + JQ1 (0.5 μM) or vehicle control for 48 hours. (**H**) Schematic of experimental model to assess immunomodulatory role of UPS cell-derived decellularized extracellular matrix (dECM). (**I**) Representative widefield images and quantification of ColVI deposition in dECM from KP cells expressing control or *Yap1*-targeting shRNAs. One-way ANOVA with Dunnett's (vs. shScr). Scale bars = 25 μM. Image brightness and contrast were adjusted for publication. (**J**) Quantification and representative contour plots showing IFNγ and TNFα co-expression in $CD44^{+}CD8^{+}$ T cells incubated on dECMs from control and shYap1-expressing KP cells. Each point represents T cells isolated from an individual mouse. One-way ANOVA with Dunnett's (vs. shScr). The shScr plot and data are identical to those in **Figure 5A** (performed in the same experiment).

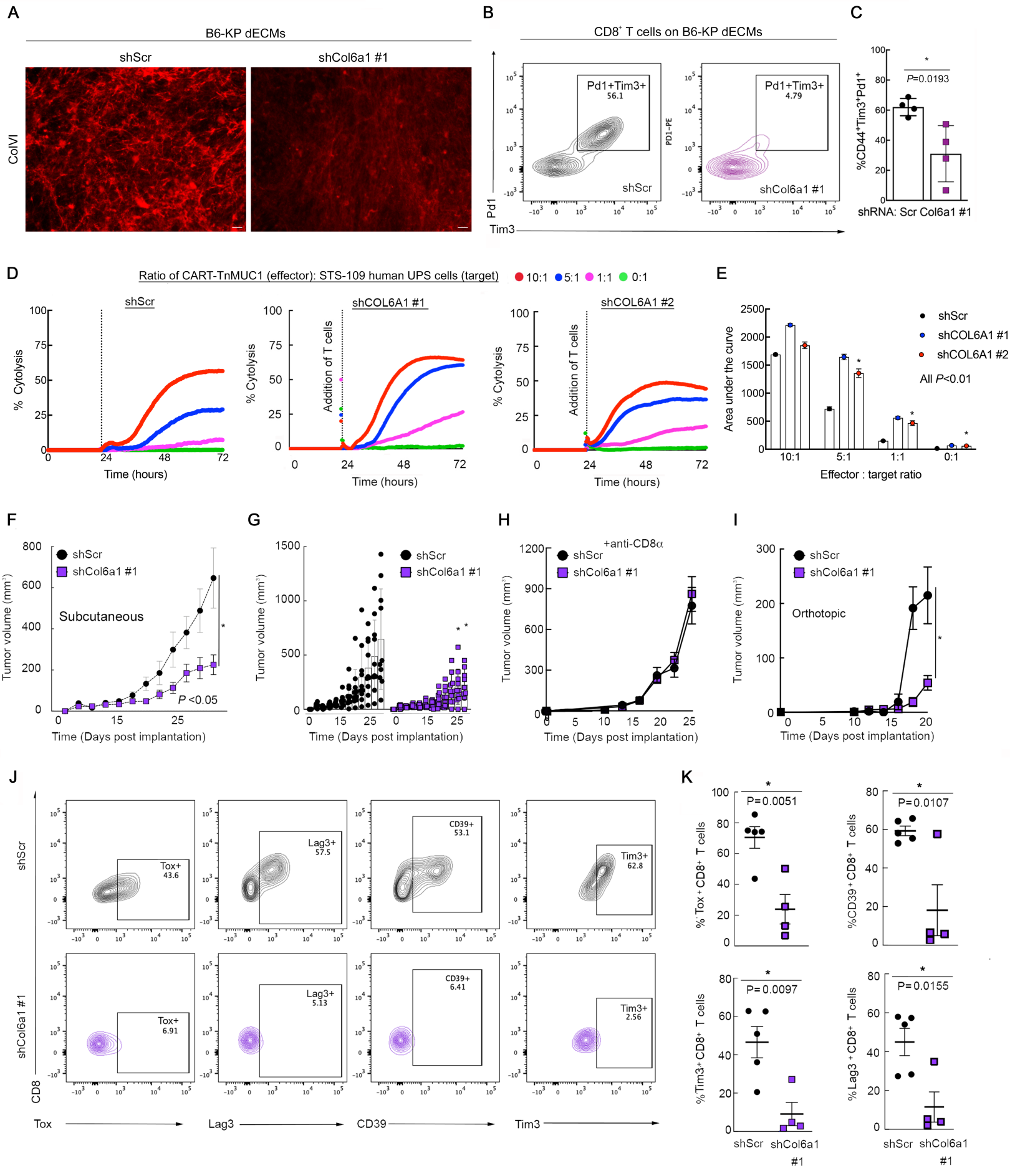
A
B6-KP dECMs
shScr
shCol6a1 #1
ColVI
B
CD8+ T cells on B6-KP dECMs
Pd1+Tim3+
56.1
shScr
Pd1+Tim3+
4.79
shCol6a1 #1
PD1-PE
Pd1
Tim3
C
*
P=0.0193
%CD44+Tim3+Pd1+
shRNA: Scr Col6a1 #1
D
Ratio of CART-TnMUC1 (effector): STS-109 human UPS cells (target)
10:1 5:1 1:1 0:1
shScr
shCOL6A1 #1
shCOL6A1 #2
% Cytolysis
Addition of T cells
Time (hours)
E
Area under the curve
shScr
shCOL6A1 #1
shCOL6A1 #2
All P<0.01
10:1
5:1
1:1
0:1
Effector : target ratio
F
shScr
shCol6a1 #1
Subcutaneous
Tumor volume (mm3)
P <0.05
Time (Days post implantation)
G
shScr
shCol6a1 #1
Tumor volume (mm3)
Time (Days post implantation)
H
+anti-CD8α
shScr
shCol6a1 #1
Tumor volume (mm3)
Time (Days post implantation)
I
shScr
shCol6a1 #1
Orthotopic
Tumor volume (mm3)
Time (Days post implantation)
J
shScr
shCol6a1 #1
CD8
Tox+
43.6
Lag3+
57.5
CD39+
53.1
Tim3+
62.8
Tox+
6.91
Lag3+
5.13
CD39+
6.41
Tim3+
2.56
Tox
Lag3
CD39
Tim3
K
P=0.0051
% Tox+CD8+ T cells
P=0.0107
%CD39+CD8+ T cells
P=0.0097
% Tim3+CD8+ T cells
P=0.0155
%Lag3+CD8+ T cells
shScr
shCol6a1 #1

Figure 3. ColVI in the UPS TME promotes CD8$^+$ T cell dysfunction. (**A**) Representative widefield images of ColVI immunofluorescence in dECMs generated from control and shCol6a1-expressing B6-KP cells. Scale bar = 20 μm. Brightness and contrast were adjusted for publication. (**B**) Representative contour plots and (**C**) quantification of Pd1 and Tim-3 co-expression in CD44$^+$CD8$^+$ T cells incubated on dECM derived from control or shCol6a1 KP cells. (**D**) Average longitudinal cytolysis of shScr or shCOL6A1-expressing human STS-109 UPS cells co-cultured with CART-TnMUC1 cells from 3 independent human donors (n = 2 for shCOL6A1 #1). Points for individual replicates overlap. Measurements indicate % target cell (UPS cell) cytolysis. (**E**) Quantification of area-under-the-curve from **D**; one-way ANOVA with Dunnett's (vs. shScr) for each ratio. In **D, E**, shScr data are identical to those in **Fig. 1J** (performed in the same experiment). (**F**) Tumor growth curves from subcutaneous (flank) syngeneic transplant of 3 x 10^4 B6-KP cells in Matrigel expressing control or *Col6a1*-targeting shRNAs in syngeneic C57BL/6 mice. Two-way ANOVA. (**G**) Individual tumors from **F**. (**H**) Tumor growth curves depicting subcutaneous (flank) syngeneic transplant of 5 x 10^5 KP cells (SKPY42.1 cell line) expressing control or *Col6a1*-targeting shRNAs in C57BL/6 mice treated with α-CD8α every three days. (**I**) Tumor growth curves depicting syngeneic orthotopic transplant (into the gastrocnemius muscle) of 2.5 x 10^5 KP cells (SKPY42.1 cell line) expressing control or *Col6a1*-targeting shRNAs in C57BL/5 mice. Two-way repeated-measures ANOVA, SEM. (**J, K**) Representative contour plots (**J**) and quantification (**K**) of T cell dysfunction markers in CD8$^+$ T cells from control and shCol6a1 orthotopic tumors from **I**. Each point in **K** represents an individual tumor. Two-tailed unpaired t-tests.

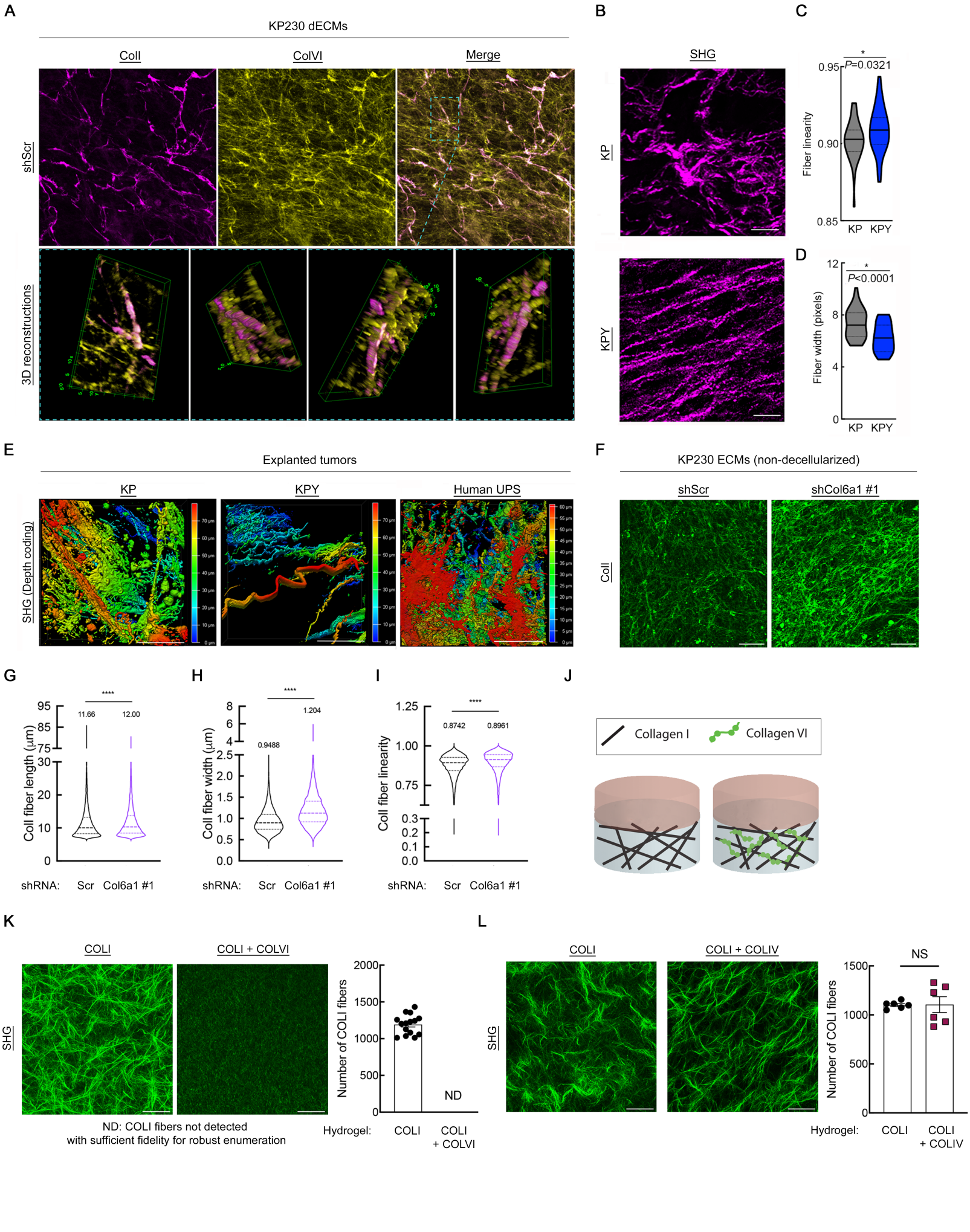
A
KP230 dECMs
ColI
ColVI
Merge
shScr
3D reconstructions
B
SHG
KP
KPY
C
*
P=0.0321
Fiber linearity
0.95
0.90
0.85
KP
KPY
D
*
P<0.0001
Fiber width (pixels)
12
8
4
0
KP
KPY
E
Explanted tumors
KP
KPY
Human UPS
SHG (Depth coding)
F
KP230 ECMs (non-decellularized)
shScr
shCol6a1 #1
ColI
G
****
11.66
12.00
Coll fiber length (μm)
95
85
75
30
20
10
0
shRNA:
Scr
Col6a1 #1
H
****
1.204
0.9488
Coll fiber width (μm)
8
6
4
2.5
2.0
1.5
1.0
0.5
0.0
shRNA:
Scr
Col6a1 #1
I
****
0.8742
0.8961
Coll fiber linearity
1.25
1.00
0.75
0.3
0.2
0.1
0.0
shRNA:
Scr
Col6a1 #1
J
Collagen I
Collagen VI
K
COLI
COLI + COLVI
SHG
Number of COLI fibers
2000
1500
1000
500
0
ND
Hydrogel:
COLI
COLI + COLVI
ND: COLI fibers not detected
with sufficient fidelity for robust enumeration
L
COLI
COLI + COLIV
SHG
NS
Number of COLI fibers
1500
1000
500
0
Hydrogel:
COLI
COLI + COLIV

Figure 4. ColVI interacts with and remodels ColI in the UPS TME. (**A**) Representative confocal micrographs (maximum-intensity Z-projections) and 3D reconstructions showing ColI and ColVI co-immunofluorescence in KP cell-derived dECMs. Scale bar = 100 μM (**B**) Representative multiphoton second-harmonic generation (SHG) images (maximum-intensity Z-projections) of KP and KPY tumor sections. Scale bars = 50 μM. (**C, D**) Violin plots of CT-FIRE analysis of images from **B**. Mean fiber width and linearity were plotted for ≥5 separate fields (n = 5 mice per genotype); two-tailed unpaired t-test. (**E**) Representative depth-coded SHG images of human UPS, KP, and KPY explanted live tumors. Red = SHG signal farthest from the objective/greatest relative tissue depth, blue = SHG signal closest to the objective/shallowest relative tissue depth. Scale bars = 50 μM. (**F**) Representative confocal micrographs (maximum-intensity Z-projections) of extracellular ColI immunofluorescence in ECMs (non-decellularized) generated from control and shCol6a1 KP cells. Scale bars = 50 μM. (**G-I**) Violin plots depicting CT-FIRE analysis of images in **F**. Fiber length (**G**), width (**H**), and linearity (**I**) were plotted from 7 independent fields across multiple dECMs per condition. Numbers above violin plots indicate means. Thick and thin dotted lines within the shapes denote medians and quartile 1/3, respectively. (**J**) Schematic of in vitro hydrogel system to assess how purified COLVI impacts purified COLI structure/organization. (**K**) Representative SHG images (maximum-intensity Z-projections with 2x optical zoom) and quantification of COLI fiber number in COLI-alone and COLI + COLVI hydrogels. Scale bars = 50 μM. (**L**) Representative SHG images (maximum-intensity Z-projections with 2x optical zoom) and quantification of COLI fiber number in COLI-alone and COLI + COLIV hydrogels. Scale bars = 50 μM. For **K-L**, quantification was performed for ≥6 independent fields across multiple hydrogels per condition. Brightness and contrast of all micrographs in **Figure 4** were adjusted for publication.

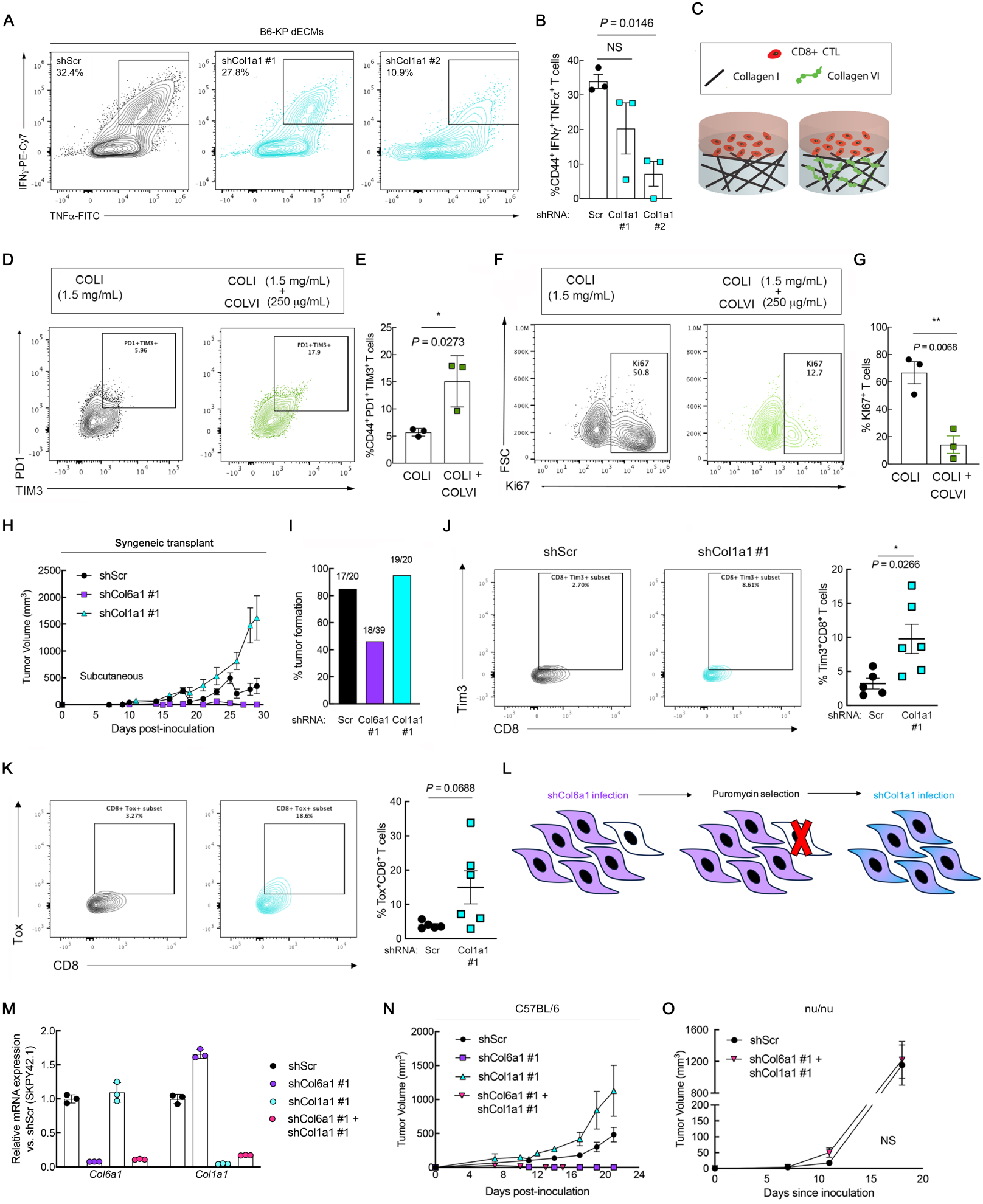
A
B6-KP dECMs
shScr
32.4%
shCol1a1 #1
27.8%
shCol1a1 #2
10.9%
IFNγ-PE-Cy7
TNFα-FITC
B
P = 0.0146
NS
%CD44+ IFNγ+ TNFα+ T cells
shRNA: Scr Col1a1 #1 Col1a1 #2
C
CD8+ CTL
Collagen I
Collagen VI
D
COLI (1.5 mg/mL)
COLI (1.5 mg/mL) + COLVI (250 μg/mL)
PD1+TIM3+ 5.96
PD1+TIM3+ 17.9
PD1
TIM3
E
*
P = 0.0273
%CD44+ PD1+ TIM3+ T cells
COLI
COLI + COLVI
F
COLI (1.5 mg/mL)
COLI (1.5 mg/mL) + COLVI (250 μg/mL)
Ki67 50.8
Ki67 12.7
FSC
Ki67
G
**
P = 0.0068
% Ki67+ T cells
COLI
COLI + COLVI
H
Syngeneic transplant
shScr
shCol6a1 #1
shCol1a1 #1
Subcutaneous
Tumor Volume (mm3)
Days post-inoculation
I
17/20
18/39
19/20
% tumor formation
shRNA: Scr Col6a1 #1 Col1a1 #1
J
shScr
shCol1a1 #1
CD8+ Tim3+ subset 2.70%
CD8+ Tim3+ subset 8.61%
Tim3
CD8
*
P = 0.0266
% Tim3+CD8+ T cells
shRNA: Scr Col1a1 #1
K
CD8+ Tox+ subset 3.27%
CD8+ Tox+ subset 18.6%
Tox
CD8
P = 0.0688
% Tox+CD8+ T cells
shRNA: Scr Col1a1 #1
L
shCol6a1 infection
Puromycin selection
shCol1a1 infection
M
Relative mRNA expression vs. shScr (SKPY42.1)
Col6a1
Col1a1
shScr
shCol6a1 #1
shCol1a1 #1
shCol6a1 #1 + shCol1a1 #1
N
C57BL/6
shScr
shCol6a1 #1
shCol1a1 #1
shCol6a1 #1 + shCol1a1 #1
Tumor Volume (mm3)
Days post-inoculation
O
nu/nu
shScr
shCol6a1 #1 + shCol1a1 #1
NS
Tumor Volume (mm3)
Days since inoculation

Figure 5. ColVI-mediated CD8$^+$ T cell dysfunction is restored in the presence of ColI. (**A**) Representative flow cytometry plots and (**B**) quantification of IFNγ and TNFα co-expression in CD44$^+$CD8$^+$ T cells incubated on dECMs from control or shCol1a1 KP cells. Each point: T cells from an individual mouse. One-way ANOVA with Dunnett's vs. shScr. The shScr plot and data are identical to those in **Figure 2J** (performed in the same experiment). (**C**) Schematic of in vitro hydrogel system to test how ColI impacts ColVI-mediated CD8$^+$ T cell dysfunction. CTL = cytotoxic T lymphocyte. (**D, E**) Representative flow cytometry plots (**D**) and quantification (**E**) of activated human CD8$^+$CD44$^+$ T cells showing TIM-3 and PD1 co-expression after incubation on hydrogels containing purified COLI with or without purified COLVI. Two-tailed unpaired t-test. (**F, G**) Representative flow cytometry plots (**F**) and quantification (**G**) of KI67 in activated human CD8$^+$CD44$^+$ T cells cultured as in **D, E**. Two-tailed unpaired t-test. (**H**) Tumor growth curves from subcutaneous (flank) syngeneic transplant of 5 x 10^5 KP cells (SKPY42.1 cell line) expressing control, *Col6a1*, or *Col1a1*-targeting shRNAs in C57BL/6 mice. Data are from two independent experiments (total n = 20 for shScr and shCol1a1; n = 39 for shCol6a1). (**I**) Tumor formation rates from **H**. (**J, K**) Representative contour plots and quantification of Tim-3 (**J**) and Tox (**K**) expression in CD8$^+$ T cells in tumors from **H**. Each point represents an individual tumor. Two-tailed unpaired t-test with Welch correction. (**L**) Schematic depicting strategy for depleting *Col6a1* and *Col1a1* in the same UPS cell population. (**M**) Validation of *Col6a1* and *Col1a1* expression in UPS cells from **L** (SKPY42.1 cell line). Technical replicates. (**N, O**) Tumor growth curves from subcutaneous syngeneic transplant of 1 x 10^6 KP cells (SKPY42.1 cell line) from **M** in C57BL/6 (**N**) and nu/nu (**O**) mice.

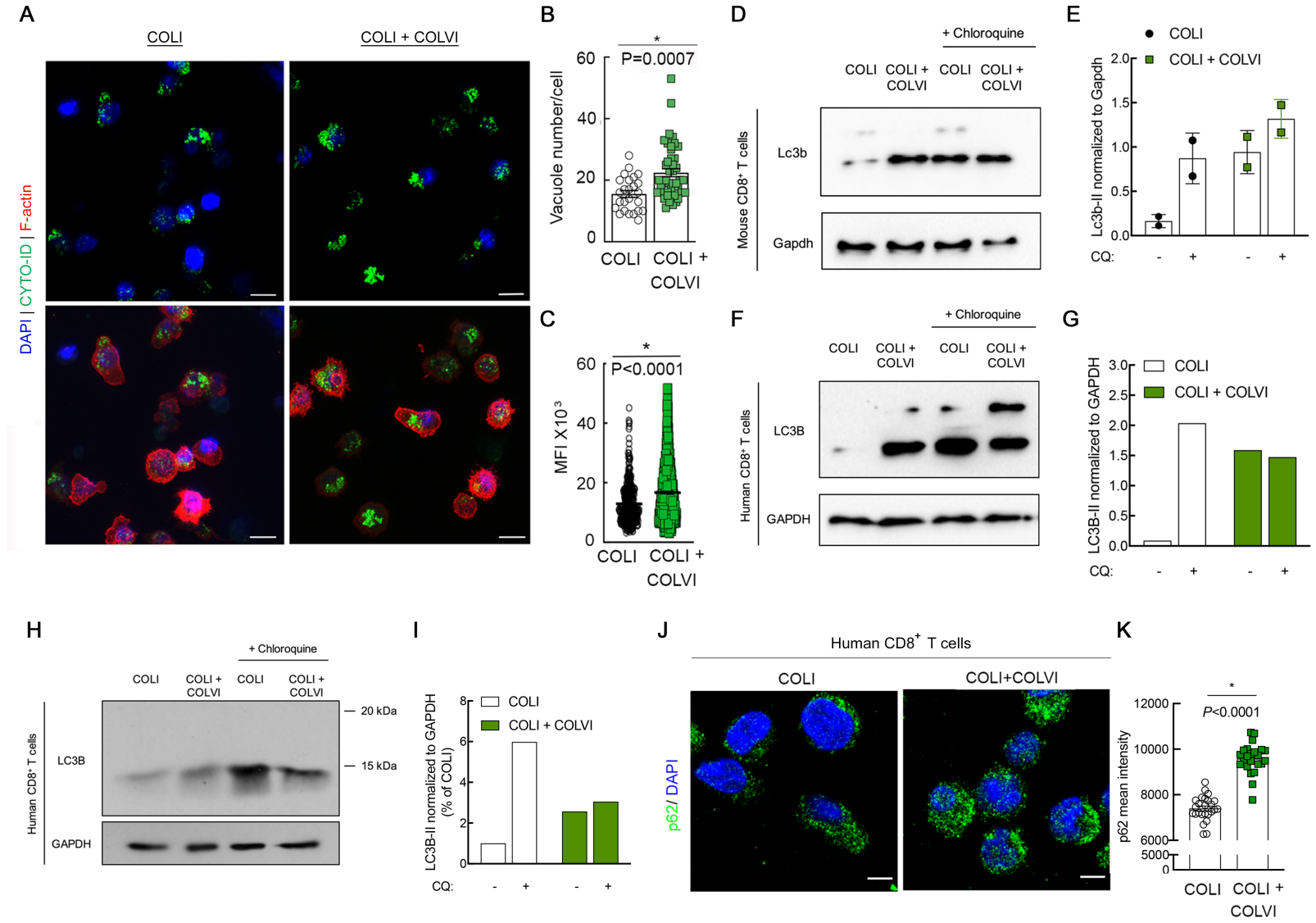
A
COLI
COLI + COLVI
DAPI | CYTO-ID | F-actin
B
Vacuole number/cell
P=0.0007
COLI
COLI + COLVI
C
MFI X10³
P<0.0001
COLI
COLI + COLVI
D
+ Chloroquine
COLI
COLI + COLVI
COLI
COLI + COLVI
Mouse CD8+ T cells
Lc3b
Gapdh
E
COLI
COLI + COLVI
Lc3b-II normalized to Gapdh
CQ:
F
+ Chloroquine
COLI
COLI + COLVI
COLI
COLI + COLVI
Human CD8+ T cells
LC3B
GAPDH
G
COLI
COLI + COLVI
LC3B-II normalized to GAPDH
CQ:
H
+ Chloroquine
COLI
COLI + COLVI
COLI
COLI + COLVI
Human CD8+ T cells
LC3B
GAPDH
20 kDa
15 kDa
I
COLI
COLI + COLVI
LC3B-II normalized to GAPDH (% of COLI)
CQ:
J
Human CD8+ T cells
COLI
COLI+COLVI
p62/ DAPI
K
P<0.0001
p62 mean intensity
COLI
COLI + COLVI

Figure 6. ColVI disrupts CD8$^+$ T cell autophagic flux. (**A-C**) Visualization (**A**) and quantification (**B, C**) of autophagosomes in CD8$^+$ human T cells cultured on hydrogels containing purified COLI with or without purified COLVI. Two-tailed unpaired t-test. (**D, E**) Western blot (**D**) and quantification (**E**) of Lc3b-II expression in murine CD8$^+$ T cells cultured on purified COLI-containing hydrogels in the presence or absence of purified COLVI, with or without chloroquine (CQ) treatment. Two-tailed unpaired t-test. n = 2. SD. (**F, G**) Western blot (**F**) and quantification (**G**) of LC3B-II expression in human CD8$^+$ T cells cultured on purified COLI-containing hydrogels in the presence or absence of purified COLVI, with or without CQ treatment. (**H, I**) Western blot (**H**) and quantification (**I**) of LC3B-II expression in human CD8$^+$ T cells cultured on purified COLI-containing hydrogels in the presence or absence of purified COLVI, with or without CQ treatment. Molecular weight marker positions are shown to demonstrate that the single LC3B band detected in this experiment corresponds to the reported molecular weight for LC3B-II (14-16 kDa for LC3B-II vs. 16-18 kDa for LC3B-I). Samples from **F, G** and **H, I** were generated from cells from different donors, and shown separately because the analyses were conducted at different institutions using different detection methods (digital fluorescent detection vs. chemiluminescence on film). (**J, K**) Representative images (**J**) and quantification (**K**) of p62 immunofluorescence in human CD8$^+$ T cells cultured on purified COLI-containing hydrogels with or without purified COLVI. Two-tailed unpaired t-test.

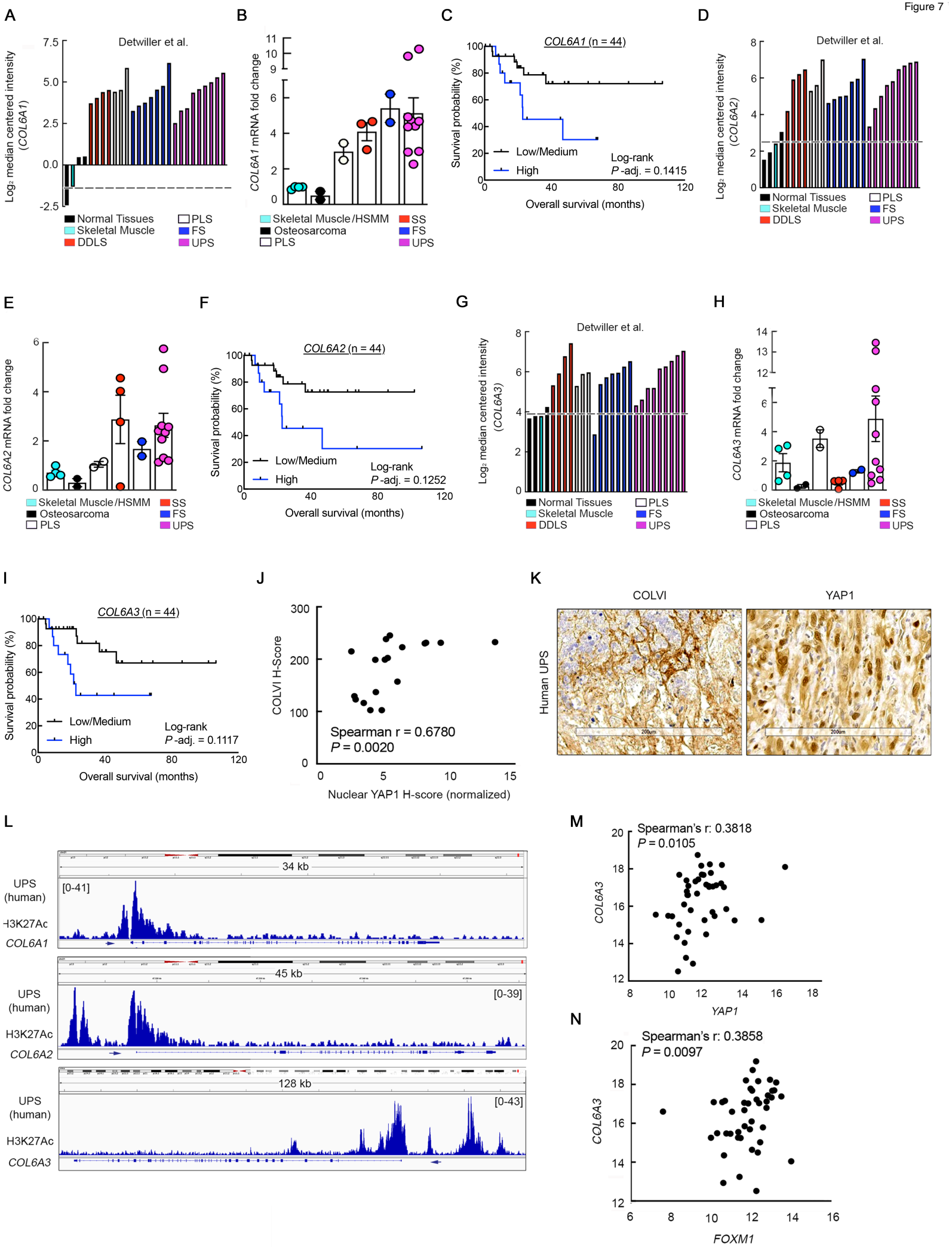
A
Detwiller et al.
Log2 median centered intensity (COL6A1)
Normal Tissues
Skeletal Muscle
DDLS
PLS
FS
UPS
B
COL6A1 mRNA fold change
Skeletal Muscle/HSMM
Osteosarcoma
PLS
SS
FS
UPS
C
COL6A1 (n = 44)
Survival probability (%)
Low/Medium
High
Log-rank
P -adj. = 0.1415
Overall survival (months)
D
Detwiller et al.
Log2 median centered intensity (COL6A2)
E
COL6A2 mRNA fold change
F
COL6A2 (n = 44)
Log-rank
P -adj. = 0.1252
G
Detwiller et al.
Log2 median centered intensity (COL6A3)
H
COL6A3 mRNA fold change
I
COL6A3 (n = 44)
Log-rank
P -adj. = 0.1117
J
COLVI H-Score
Spearman r = 0.6780
P = 0.0020
Nuclear YAP1 H-score (normalized)
K
COLVI
YAP1
Human UPS
200um
L
34 kb
UPS (human)
[0-41]
H3K27Ac
COL6A1
45 kb
[0-39]
COL6A2
128 kb
[0-43]
COL6A3
M
Spearman's r: 0.3818
P = 0.0105
COL6A3
YAP1
N
Spearman's r: 0.3858
P = 0.0097
FOXM1

Figure 7. YAP1 and COLVI expression/activity are correlated in human UPS tumors. (**A**) *COL6A1* gene expression levels in specimens from the Detwiller sarcoma dataset (Oncomine) (61). DDLS = dedifferentiated liposarcoma, PLS = pleomorphic liposarcoma, FS = fibrosarcoma. (**B**) qRT-PCR analysis of *COL6A1* expression in human sarcoma and normal skeletal muscle tissue specimens (Hospital of the University of Pennsylvania; HUP). PLS = pleomorphic liposarcoma, SS = synovial sarcoma, FS = fibrosarcoma. (**C**) Kaplan-Meier overall survival curves of UPS patients in TCGA-SARC stratified by intratumoral *COL6A1* gene expression levels. (**D**) *COL6A2* gene expression levels in specimens from the Detwiller sarcoma dataset. (**E**) qRT-PCR analysis of *COL6A2* expression in human sarcoma and normal skeletal muscle tissue specimens (HUP). (**F**) Kaplan-Meier overall survival curves of UPS patients in TCGA-SARC stratified by intratumoral *COL6A2* gene expression levels. (**G**) *COL6A3* gene expression levels in specimens from the Detwiller sarcoma dataset. (**H**) qRT-PCR analysis of *COL6A3* expression in human sarcoma and normal skeletal muscle tissue specimens (HUP). (**I**) Kaplan-Meier overall survival curves of UPS patients in TCGA-SARC dataset stratified by intratumoral *COL6A3* gene expression levels. For **C**, **F**, and **I**, tertiles (low, medium, high) represent 1/3 of patients. (**J**) Correlation of COLVI and nuclear YAP1 immunostaining in UPS tumor specimens (HUP). Each point represents an individual specimen. (**K**) Representative IHC images from **J**. Scale bar = 200 μm. (**L**) Publicly available ChIP-seq data (GSE97295) of *COL6A1*, *COL6A2*, and *COL6A3* promoter H3K27 acetylation in human UPS samples (HUP). (**M, N**) Correlation of *YAP1* with *COL6A3* (**M**) and *FOXM1* (**N**) gene expression in UPS tumors from TCGA-SARC.

A

COLVI expression score: associations with patient characteristics and tumor clinicopathologic features

		n (%)	Mean H-score (95% CI)	*P-value*[1]	Holm's α[2]	*P*- adj.[3]
Histology						
	UPS (REF.)	11 (15.71)	88.52 (17.99)			
	Leiomyosarcoma	9 (12.86)	42.89 (9.78)	**0.0003**	0.0071	0.0089
	Liposarcoma	17 (24.29)	87.69 (11.58)	0.9360	0.0500	0.9777
	Neurilemmoma	12 (17.14)	60.69 (18.90)	0.0140	0.0125	0.0765
	Neurofibroma	3 (4.29)	30.83 (15.85)	**0.0013**	0.0083	0.0097
	Other[4]	9 (12.86)	60.86 (19.37)	0.0228	0.0167	0.1070
	Rhabdomyosarcoma	5 (7.14)	81.17 (21.46)	0.6072	0.0250	0.7430
	Synovial sarcoma	4 (5.71)	38.88 (11.69)	**0.0020**	0.0100	0.0031
Age (y)						
	> 50 (REF.)	36 (51.43)	69.89 (10.67)			
	≤ 50	34 (48.57)	66.60 (10.46)	0.6687	N/A	0.8950
Grade[5]						
	G1-G2 (REF.)	30 (44.12)	55.51 (9.36)			
	G3-G4	38 (55.88)	77.87 (10.32)	0.0013	N/A	0.0197
Stage[5]						
	I (REF.)	18 (26.47)	60.64 (12.26)			
	II	18 (26.47)	67.62 (15.54)	0.5115	0.05	0.2414
	III	32 (47.06)	74.66 (11.51)	0.1385	0.025	0.1093

B

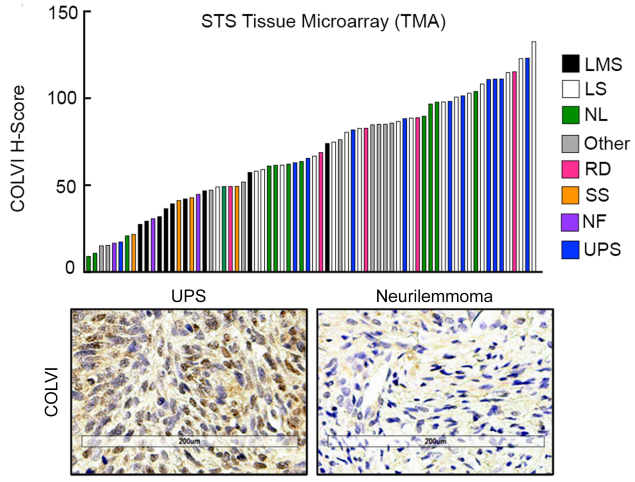

C

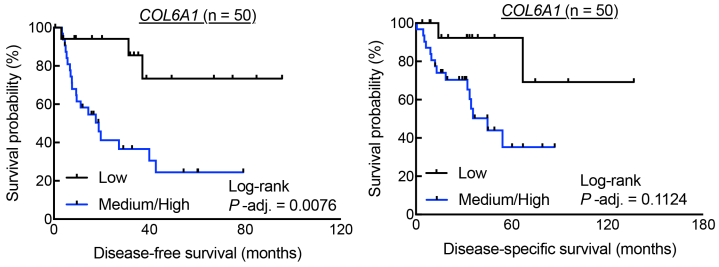

D

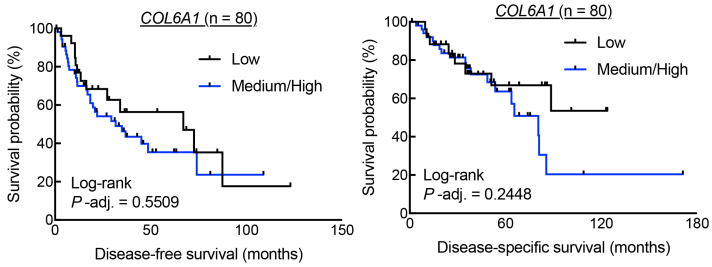

E

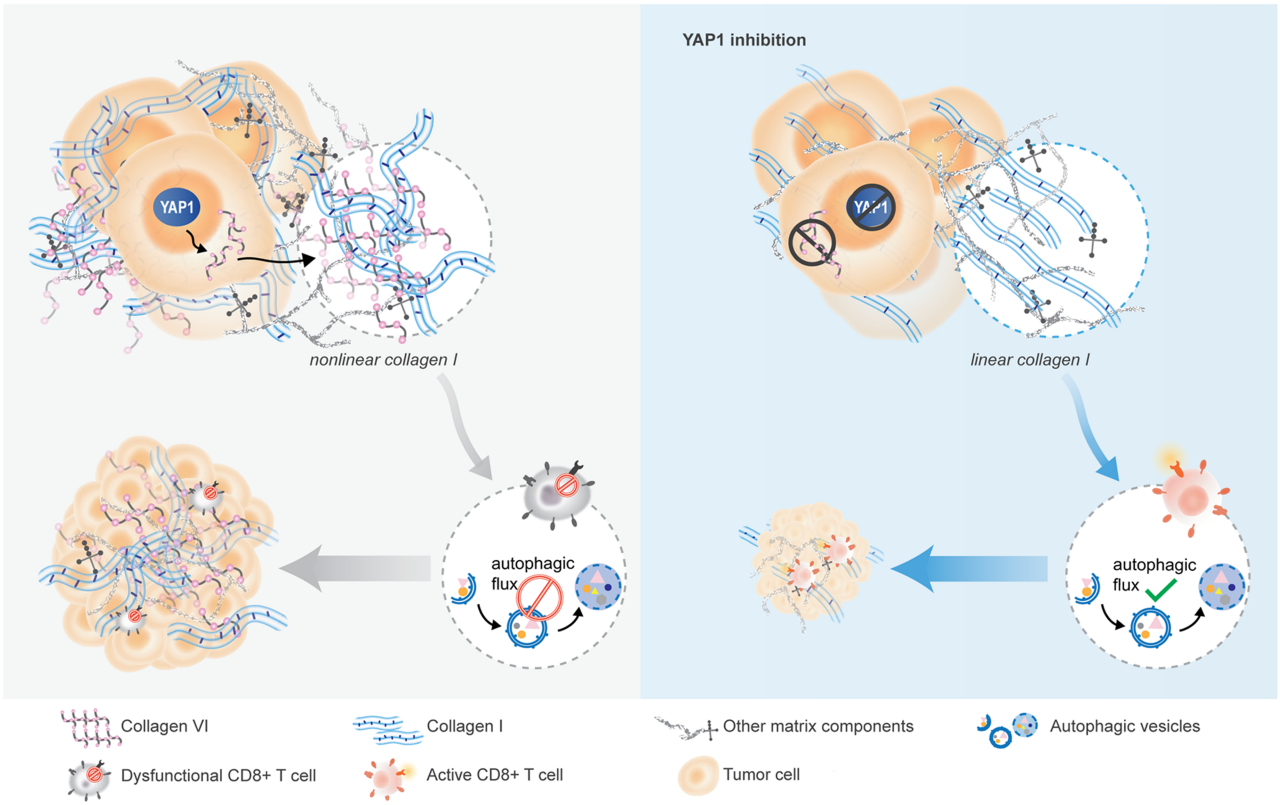

Figure 8. COLVI expression in the microenvironments of UPS and other soft-tissue sarcoma subtypes. (**A**) Association of IHC-based COLVI expression score with tumor subtype and clinicopathologic features. Sarcoma tissue microarray (TMA). [1]Univariate linear models. [2]In univariate analyses, the Holm-Bonferroni adjustment for multiple comparisons was performed for demographic or clinicopathologic variables with greater than two levels, with $\alpha = 0.05$. Results are considered statistically significant (bold text) if the univariate *P*-value is smaller than the corresponding Holm's alpha. [3]Fully adjusted model (age, grade, stage, and histology). Correction for multiple comparisons was not performed due to insufficient statistical power. [4]Includes 2 alveolar soft part sarcomas, 1 epithelioid hemangioendothelioma, 1 fibroma, 1 glomus tumor, 1 hemangioendothelial sarcoma, 1 hemangiopericytoma, 1 osteosarcoma, and 1 tenosynovial giant cell tumor. [5]Excludes two benign cases. (**B**) Waterfall plot depicting IHC-based COLVI expression scores in individual tumors from **A**. LMS = leiomyosarcoma; LS = liposarcoma, NL = neurilemmoma, RD = rhabdomyosarcoma, SS = synovial sarcoma, NF = neurofibroma. "Other" as described in **A**. Representative images of UPS and neurilemmoma are also shown. (**C, D**) Kaplan-Meier disease-free and disease-specific survival curves of (**C**) dedifferentiated liposarcoma and (**D**) leiomyosarcoma patients in TCGA-SARC stratified by *COL6A1* gene expression. Tertiles (low, medium, high) represent 1/3 of patients. (**E**) Model depicting study findings.